# Fuzzy typological (re)arrangement. A prototype of rethinking the typology of Roman tablewares from Sagalassos, southwest Anatolia

Danai Kafetzaki[*,1,2], Jeroen Poblome[1], Jan Aerts[3]

[1] Sagalassos Archaeological Research Project, KU Leuven, Leuven, Belgium
[2] Center for Statistics, Data Science Institute, UHasselt, Hasselt, Belgium
[3] KU Leuven, Leuven Statistics Research Centre (LStat), Leuven, Belgium
[*] Corresponding author.

## Abstract

Organizing archaeological artefacts under a conceptual system is part and parcel of archaeological research. As an abundant material category, pottery artefacts classified in an effective typological model provide a rich source of information for the discipline. However, building a typological model from scratch, as well as maintaining it, often represents a challenge. To support archaeological research, automated methods are increasingly utilized in sustaining classification models. Yet, there is potential for advancement in creating, rethinking and updating typological arrangements by means of digital, label-driven or data-driven algorithmic approaches. In this paper, we take a step towards fulfilling this potential while highlighting the fuzziness involved in typological arrangements. We present a complete research pipeline of pottery form quantification, fuzzy type description and fuzzy type definition which is in principle applicable to any typological model. The methodological pipeline is implemented, first, in rim segments to algorithmically construct polythetic rim descriptors, second, in complete profiles to algorithmically connect the global form with the attributed functional class, and third, in types to investigate within-class form variation and its chronological relevance. This paper provides tools to formalize the ambivalence of typological classification using fuzzy logic, and revisit the theoretical model to investigate the vagueness of belonging to a class based on morphological aspects of pottery profiles.

**Keywords** fuzzy logic; algorithmic typology; geometric morphology; shape analysis; visual analytics; Roman pottery

## Introduction

Pottery analysis structures archaeological research problems and supports the study of a variety of archaeological research topics. This presupposes an underlying conceptual system based on the organization of material culture into distinct classes. (Read, 2007; Rice, 2015). There are many ways to arrange pottery materials, including technology used, morphology, function, and style. Most often, technological and morphological aspects form the basis of classifying pottery. As far as technology is concerned, methods quite often revolve around the study of clay fabrics, applying concepts such as *chaîne opératoire*, object biography or entanglement (Duistermaat, 2016). Morphological studies contribute to several levels in pottery typologies through empirical form quantification and classification strategies but also provide access to several interpretative directions to reflect on less tangible aspects, such as chronological, cultural, social, or functional properties (Albero et al., 2016). Devising a typological model is a complex task and its impact in archaeological interpretations can be significant, especially when dealing with the abundance of pottery material, which has currently seen much digital advancement (Karl et al., 2022). Different interpretations of a single well-defined typological model are considered complementary (Albero et al., 2016) while the concept of multivocality (Banning, 2020) highlights that equally plausible interpretations and therefore also classifications can be suggested by material specialists, and all are accepted as long as there is theoretical basis (Adams & Adams, 1991).

The concept of typological arrangement traditionally falls into one of two categories: classification or *definitive* approaches and grouping or *descriptive* approaches (Dunnell, 1971; Banning, 2020). Typological arrangements of both sorts have been applied algorithmically in archaeological data. In the definitive approach, one of the early applications, is the taxonomic classification of Whallon (1972) where association analysis using chi-square tests on contingency tables was employed to propose a tree algorithm for typological arrangement in Owasco pottery. Read (2009) applied paradigmatic classification on contingency tables using a log-linear model for morphological characteristics of Castanet-A Paleolithic end-scrappers. From the advent of Artificial

Intelligence in all fields of research, several works on automatic classification of pottery by means of predictive modelling were published (Kampel & Sablatnig, 2007; Tyukin et al., 2018; Cintas et al., 2020; Anichini et al., 2021; Gualandi et al., 2021; Navarro et al., 2021; Lucena et al., 2016, 2017; Pawlowicz & Downum, 2021). These methods were applied to a range of data, including Roman tableware, Roman amphorae, Iberian wheel-made pottery and Tusayan White Ware from Northeast Arizona.

An early application of the descriptive approach by Green (1975) retrieved fifty-four material attributes using a standardized coding procedure, which were used to perform clustering analysis. Clustering results were compared to the labels of the traditional typology for generating and testing hypotheses between numeric and traditional methods. In another application, pottery sherds from Czersk Castle in Poland were clustered according to size and chemical composition (Kobylinski & Buko, 1992). Another label-free approach was discussed by Christmas and Pitts (2018) for Roman pottery in Britain. The authors analyzed images of ceramic vessel by segmenting them in four regions and taking measures for height and width, centroid, volume, circularity and rectangularity. They then performed k-means clustering and compared with the assigned class using a confusion matrix. In the work of Van Der Maaten et al. (2005), similarity between pottery profile finds in the Netherlands was measured using shape contexts and thin plate splines. The quantified data were visualized with t-SNE and affinity propagation clustering was used to define groups. Karasik and Smilansky (2011) followed an approach using Principal Component Analysis, clustering and Discriminant Analysis of early Iron Age pottery at Tel Dor. Gansell et al. (2014) proposed stylistic clusters of ivory carvings based on a combination of descriptive and morphological data. The authors used a mixture model for computing clusters and visualized the clusters using a network graph. Mutual Information was computed to rank the predictive attributes with respect to the clustering result. Finally, Parisotto et al. (2022) presented hierarchical clustering of neural network features from the latent representation space of a stacked sparse autoencoder (SSAE) network as a typological arrangement method for pottery in ROman COmmonware POTtery (ROCOPOT) database.

Although algorithmic approaches have been increasingly applied in typological arrangement, they usually do not treat the vagueness involved in the internal logic of a typological arrangement as a requested aspect of the algorithmic model output. This goes against the realization that hard boundaries do not naturally occur in material culture (Adams & Adams, 1991; Hermon et al., 2004). In principle, groups intersect and overlap (Banning, 2020; Orton et al., 2013) and the development of a typological arrangement can be considered a cognitive task resulting in a folk taxonomy based on semantic change and similarities between material, utilizing prototypes and grading (Kempton, 1981). These less rigid definitions match the cognitive task of building and maintaining a typological model and utilizing prototypes as reference points as well as non-prototype members to perform categorization, as in tasks that dealt with judging perceptual distances in (Rosch, 1975). Such information is not explicitly captured in traditional typological classes and the commonly used hard- and single-valued classes eliminate relationships between individual profiles and to an extent also between classes.

One way to model the information vagueness, is to employ *fuzzy logic*, for which the underlying rationale was first introduced by A. L. Zadeh (1965) and remains in use today with applications in several areas (Kahraman et al., 2016). The value of fuzzy logic has already been widely discerned in archaeology (Adams & Adams, 1991; Banning, 2020; Barceló, 1996; Niccolucci & Hermon, 2015; Orton, 1982). Fuzzy logic applications in archaeological data have been focusing on storing and retrieving information from databases, as in the works of Niccolucci and colleagues (2001), who created fuzzy SQL expressions for fuzzy age, gender and chronology of burials data in land properties, as well as in the work of Martin-Rodilla and Gonzalez-Perez (2019) who also discussed the concept of information vagueness and proposed a non-relational query system that allows managing vague information. In combining information using fuzzy logic, Runz et al. (2007) proposed the fuzzy Hough transform to merge the fuzzy representation of three sources of information, namely localization, orientation, and temporal interpretation of excavation points to map Roman streets. Migliorini et al. (2022) proposed a pipeline for merging and mining fuzzy temporal information of archaeological artefacts provided by different researchers while retaining data provenance. They implemented this pipeline in a study of the Porta Borsari, an ancient Roman gate in Verona, and an adjacent historical building. Fuzzy clustering has been exploited in a few typological arrangements, such as in the work of Calliari et al. (2001) where bricks acquired from Roman and medieval building levels in Venice were grouped based on chemical composition and geometric measures data. Harris et al. (1993) clustered countries based on demographic and socio-economic variables, while Baxter (2009) highlighted the scarcity of fuzzy clustering applications in archaeology and provided three examples of grouping artefacts based on their chemical composition. Finally, Hermon and Niccolucci (2002) were the first to assess the fuzziness of class definition in an established typology for stone tools, based on the disagreement between five different researchers who classified fifty tools of one assemblage from a protohistoric site in Israel. In this work

– as well as a later study (Hermon et al., 2004) – the ‘reliability index’ is utilized to quantify the ‘degree of confidence’ in the classification of an item, but also in a type or assemblage. A fuzzy inference system application of archaeological data is discussed in (Taheri et al., 2019), where gender determination is inferred based on burial information and measurements on bones.

From this literature review we can surmise that the suitability of fuzzy logic in archeological classification is recognized, but fuzzy logic approaches in typological arrangements of pottery remain limited. Earlier applications – which have been applied to stone tools – revolved around consensus analysis between researchers while descriptive arrangements have been implemented algorithmically with fuzzy clustering using pottery chemical data. To our knowledge, fuzzy logic has not been previously explored on algorithmic typological arrangements of *terra sigillata* based on morphological analysis.

In this paper, we aim to take a step further in algorithmically implementing aspects of theoretical typology models with fuzzy logic conventions. Our focus is on type description and type definition. In this work, we provide a methodology to include the soft-boundaries rationale in existing or developing pottery typological models, in cases where labels are already provided or when they are constructed from scratch. We provide tools for algorithmically reconstructing and rethinking pottery classes based on automatic quantification of pottery forms that allow replicable, high-dimensional comparisons, and tracking of various features simultaneously while offering potential for reflection between computational approaches and traditional material studies.

We illustrate our approach on published typological classes referring to polythetic descriptors, functional interpretation and variants within types, using morphological data retrieved automatically from technical drawings of Sagalassos Red Slip Ware. In section ‘Sagalassos Red Slip Ware: Typological model and background information’, we briefly discuss the components of the revisited typological model. Our goal is to utilize morphological characteristics while keeping properties such as fabric, culture, and space fixed, to include the fuzziness in an algorithmic typological (re)arrangement. We aim to provide centrotypes (Main, 1987) and techniques that capture the ‘continuum’ problem in typological models (Orton et al., 2013). For algorithmically proposed types, we aim to evaluate potential chronological saliences.

In ***Fig. 1***, a sketch of the various stages of the analysis is shown. The digital model first translates technical drawings into numerical data capturing pottery forms. In section ‘Shape quantification’ we discuss methods to quantify the shape of pottery profiles and we explain the approaches we apply in our data. We then compute (dis)similarity between extracted pottery forms and infer (dis)similarity between group means, as illustrated in section ‘Dissimilarity between profiles’. In section ‘Fuzzy type description’ we provide our contribution to methods for obtaining fuzzy polythetic rim descriptors and fuzzy functional descriptors using custom-made fuzzy rules. In section ‘Fuzzy type definition’ we present our approach for proposing algorithmic type-varieties using fuzzy clustering and network embedding. The analytical pipeline is dependent on the conceptual model and interacts with it, providing insights into traditional chronological modelling, class vagueness, and provenance for the causes of attributing a textual label in the fuzzy logic process. In the results section, we apply our proposal in three settings. First, we construct fuzzy rim descriptors from scratch, second, we develop fuzzy sets for the single-valued functional labels already attributed to profiles, and finally, we propose fuzzy algorithmic varieties within four selected types of the original typological model.

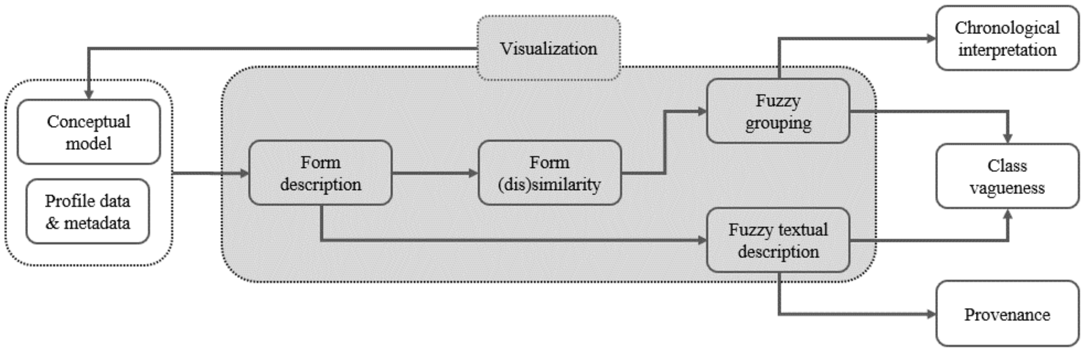


***Fig. 1*** *Sketch of the proposed digital model. Starting from the conceptual typological model and the profile data and metadata, the form of each profile is described quantitatively. Fuzzy textual description is applied directly after. To perform fuzzy grouping, we first compute the (dis)similarity between each pair of the profiles. Using visualization to access and interpret the results, each step of the process is evaluated based on the conceptual*

*model, which may inform morphological description and restart the process. The outcome provides insights on the vagueness of the typological class, highlighting typical, atypical and marginal cases. The fuzzy textual description methodology provides the means to highlight the cause and the origin of attributing a descriptor to a profile. The fuzzy grouping results are judged for potential effects on chronological interpretation.*

## Sagalassos Red Slip Ware: Typological model and background information

The archaeological site of Sagalassos is located in south-western Anatolia (Turkey) and has a long settlement history. Sagalassos emerged as an organized community by the end of the Achaemenid period (late 5th century BCE) and the site was continuously inhabited until the Middle Byzantine period (13th century CE). During Roman Imperial and Early Byzantine times ($2^{nd}$ half first century BCE – $7^{th}$ century CE) and following antecedents, a local form of tableware, named Sagalassos Red Slip Ware (SRSW) was produced in the eastern *proasteion* of the site (Poblome, 2016). SRSW forms part of a wider tradition of (eastern) sigillata and red slip wares in the Hellenistic world and later on in the Roman Empire. The term tableware refers mainly to the function of consuming food and beverages, with cups, bowls and dishes and of serving, with plates and containers. Closed shapes, including jugs and jars, were also produced in SRSW, but these are not considered in this paper (following Poblome 1999).

Following the taxonomic classification of arrangements (Dunnell, 1971; Banning, 2020), the SRSW typology is built as a descriptive arrangement and utilizes grouping methods. This type of methods provides an ideal basis for the research conducted here as it is typically based on intrinsic characteristics of the material and allows fuzziness. Diagnostic SRSW sherds are labeled based on the original typological model of 78 type-variants (Poblome, 1999) which were assigned functional characteristics described further by Poblome and Bes (2018).

To construct the typological model, mainly central tendency methods are applied. *Type-varieties* are used to group and present the material collection, named type-variants in the original typological model. Inked technical drawings and nowadays increasingly digitized versions, are collected per type-variant to showcase representative profiles and to capture the whole area the shape spans inside each type-variant.

Type-variants are accompanied by textual *polythetic descriptions* for each type-variant. Textual descriptors are, in general, suited to record complicated shapes and in published typologies, they are traditionally available in free text on the level of the type, not that of the sherd (Poblome, 1999; Hayes, 1991; Meyza, 2007). For this paper, we tabulated the textual descriptors attributed to SRSW, per type-variant and per segment of the profile: rim, wall, base; as well as global shape, grooves, decoration, and whether complete profiles are found, which other type-variant there might be similarities with, and finally miscellaneous/other. Variation in description occurs between the 78 type-variants but some individual descriptors recur. Below we present the recurring descriptors and their count in parenthesis. For the rim segment these are: thickened (40), rounded (38), plain (20), horizontally flattened (16), everted (15), vertically flattened (7). For the wall segment: convex (30), outspread (19), straight (12). For the global shape: open (63), small (17), closed (16), large (10), deep (11), shallow (9).

In addition to type-variants and polythetic descriptors, geometric measures are defined to tabulate *statistical summaries* and present histogram plots. Geometric measures usually encode shape and size features and they are collected per sherd. Poblome (1999) defined ten of these measures, referring to the rim, body, base, wall and the position of the grooves, as depicted in ***Fig. 2***.

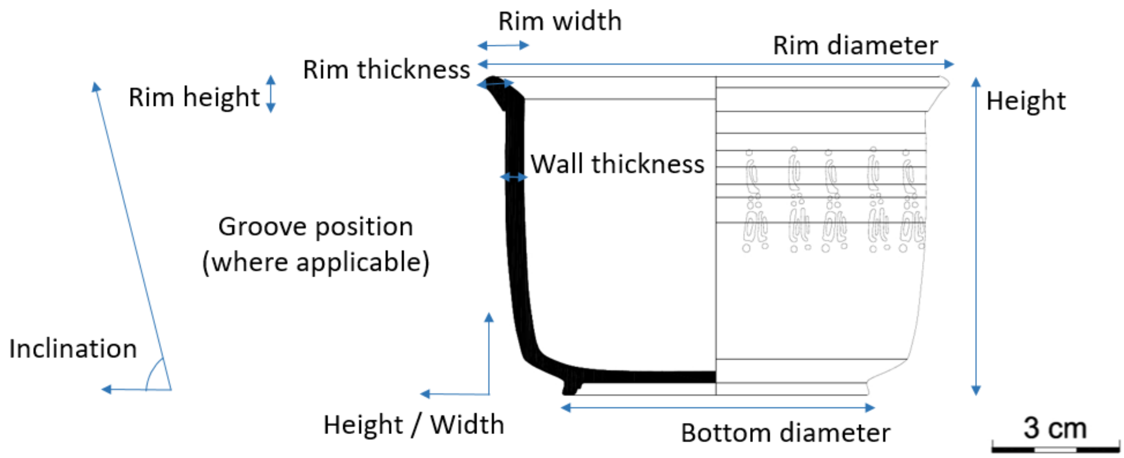


*Fig. 2* *Geometric measures collected for the original SRSW typological arrangement*

# Fuzzy algorithmic classes

We may argue that typological model building is *ab initio* an ill-posed problem, first and foremost because no unique solution exists. Even from an emic perspective, any overlap between two types causes grey areas in distinctiveness, making an absolute dichotomy impossible. Proportionately, we do not expect to provide an absolute result in the sense that this outcome is the truth from an emic perspective. We should rather consider the work proposed here as a digital method that adheres to standards of grouping arrangements in pottery analysis and respects the fuzzy boundaries rationale it exhibits.

In this section, we illustrate the methods employed to obtain digital models for polythetic rim descriptors (section 'Theory-driven fuzzy sets') and for translating SRSW functional labels to fuzzy labels (section 'Label-driven fuzzy sets') using custom-made fuzzy rule implementation. The rules are developed using geometric morphology measures described in section 'Geometric morphology measures'. Next, we illustrate the methods employed to obtain algorithmic type-varieties using fuzzy clustering and network embedding (section 'Fuzzy type definition'). Type definition is also based on shape characteristics described in section 'Shape quantification'.

## Fuzzy type description

The development of typological models using textual descriptors has long roots in archaeology, preceding the development of ontologies and controlled vocabularies such as Getty's Art & Architecture Thesaurus (AAT). AAT is a significant step towards digital transformation in the field of archaeology, and some concepts we describe in this paper are included in AAT, such as the categories of cup (ID: 300043202), bowl (ID: 300203596), dish (ID: 300042973), plate (ID: 300042973), and container (ID: 300198855) as well as the concept of rim sherd (ID: 300263317). However, two caveats need to be stated: First, the terms are not linked to the morphology of the underlying data, and second, the granularity is not of the desired level to describe pottery typological models. Polythetic descriptors are traditionally developed qualitatively following scholarly literature but also capturing the specificities of pottery morphology within research projects and their research aims. The language of the descriptors may also be different across research projects and efforts have been made to translate terms and link them to existing systems e.g. (High-Steskal et al., 2019; Anichini et al., 2020). We recognize that more work is needed to move forward in this direction and this can only be a collective effort by the field. In this paper, we add to such efforts by describing terms, some are mapped to AAT and some are not, according to the underlying morphology of the profiles and the theoretical typological model. Having such a link between polythetic descriptors and morphological characteristics could provide standardizations and guidance for attributing polythetic descriptors and in the future it could potentially enrich AAT. We provide methods that can be used to map selected terms and concepts using fuzzy logic. These methods are in general applicable to polythetic descriptors that are designed form scratch based on theory or from labels already available per sherd or vessel.

Our methods provide the possibility to highlight the provenance of the decisions and explain why a profile has the specific fuzzy label.

### The backbone of Fuzzy Logic

Fuzzy logic is highly suitable for designing polythetic descriptors because it resembles human decision-making, provides a way to solve problems by experience rather than knowledge, and deals with vague information. In contrast with Boolean logic and classical (crisp) sets, where a value can be either true or false, with fuzzy logic and fuzzy sets we can introduce shades of grey between the true and false values. In fuzzy logic, verbal (polythetic) type descriptors are treated as linguistic variables (L. A. Zadeh, 1973) which takes at least two values simultaneously, with a degree of truth associated to each value, which is called support.

The support of each value in the fuzzy variable is calculated based on if-then rules and membership functions. For the fuzzy set $\widetilde{\mathrm{A}}$, the membership function $\mu\widetilde{\mathrm{A}}(\bullet)$, is defined in the universe of discourse that spans the whole area the numeric input can take, in our case a geometric morphology measure. The shape of the membership function is application-dependent and there are several approaches for its elicitation (Bouchon-Meunier et al., 1996; Türkşen, 1991; Bilgiç & Türkşen, 2000; Dubois & Prade, 2021). In this work we define membership functions using either theoretical considerations (section 'Theory-driven fuzzy sets') or empirical probability density functions (section 'Label-driven fuzzy sets'). The membership function is connected to the output fuzzy set with if-then rules. Each if-then rule consists of the antecedent or premise and the consequent or conclusion. In the case where the antecedent has multiple parts, these are combined with a fuzzy operator: and, or, not. Assuming $\widetilde{\mathrm{A}}$, $\widetilde{\mathrm{B}}$ and $\tilde{\mathrm{C}}$ are fuzzy sets that are attributed a linguistic value, the structure of an if-then rule is the following: If $(\mathrm{x\ is\ }\widetilde{\mathrm{A}})$ and $(\mathrm{y\ is\ }\widetilde{\mathrm{B}})$ then z is $\tilde{\mathrm{C}}$. The last part of the rule (then z is $\tilde{\mathrm{C}}$) is the consequent and the previous part is the antecedent. Following the evaluation of the antecedent, an implication method is needed to apply the result to the consequent. Common implication methods employ the minimum or the product functions. In our setting, the minimum implication method is used, which clips the output fuzzy set according to the result of the antecedent. The result of each if-then rule is combined with an aggregation method, specifically, in this paper, the maximum aggregation method. The output fuzzy set thus has as many values as the linguistic variable, e.g. three values, $\tilde{C} = \left\{\frac{support_{v1}}{v1} + \frac{support_{v2}}{v2} + \frac{support_{v3}}{v3}\right\}$.

### Theory-driven fuzzy sets

This approach was used in our work to define polythetic rim descriptors. For constructing if-then rules from scratch, we followed a four-step approach. First, we collected qualitative data about the definition of polythetic descriptors, during free-form discussions and training provided from three material specialists experienced with SRSW. Then, we quantified morphological characteristics of interest to a set of geometric morphology measures, listed in section 'Geometric morphology measures'. Next, we used few of most common membership functions in fuzzy logic to associate the geometric measures with the polythetic descriptors. Finally, we evaluated our results using visualisation (see section 'User Interface'). The process was repeated until a model that resembles the conceptual model of material specialists is determined.

Common membership functions are the Gaussian, trapezoid, triangular, sigmoidal and linear functions (Pappis & Siettos, 2014). In this work, we mathematically define membership functions using either the Gaussian or the Logistic functions. The Gaussian function is $G(x;\mu,\sigma) = \exp\left(-\frac{(x-\mu)^2}{2\sigma^2}\right)$, where $\mu$ is the mean and $\sigma$ is the standard deviation. The Logistic function is $S(x;k,x_0) = \frac{1}{1+\exp(-k(x-x_0))}$, where $k$ is the logistic growth rate or steepness of the curve and $x_0$ is the x-axis value of the sigmoid midpoint. The logistic growth rate is positive for monotonically increasing functions and negative for monotonically decreasing functions.

The visualisation used to evaluate the membership functions involved in polythetic rim description included 471 SRSW rim sherds, spanning the SRSW typology.

### Label-driven fuzzy sets

This method was used to connect vessel shape with SRSW functional classes and build a digital model to translate crisp labels to fuzzy labels, based on the relationships between global vessel shape characteristics. Under this approach, the empirical probability density functions for each geometric measure per class informs the construction of membership functions. In practice, a model can be fitted for any dataset where crisp labels are provided from the material specialists and the shape quantification method is in place.

Our proposal is inspired by the reconciliation between fuzzy sets and probability which is commonly denoted as (quantitative) possibility theory and has been widely studied (L. A. Zadeh, 1978; Dubois & Prade, 1988; Klir, 1999; Dubois, 2006; Pota et al., 2013; Dubois & Prade, 2015; Angelov & Gu, 2018; Pota et al., 2018). In this work, label-driven membership functions are defined relatively to the probability density function.

To implement in our setting, first, we compute the frequency distribution of each input variable per label class. Then, we compute the empirical probability density function using kernel density estimation with Gaussian basis function and bandwidth calculated in each case according to Silverman's rule of thumb (Silverman, 1986). The resulting estimate is normalized such that the maximum likelihood is set to one, the minimum is set to zero and then the estimate is clipped at the lower and upper bound of the input *universe of discourse*. Consequently, we end up with the *membership function* in which the *support* values are drawn in parallel with the likelihood.

This choice nonetheless imposes a difficulty in the linguistic interpretation of the estimated fuzzy sets. Since we are dealing with empirical data, the shape of a membership function may be atypical, i.e. non-convex and multimodal, while a decomposed multimodal set may include a normal subset (maximum support is one) and one or more subnormal subsets (maximum support is not one). Based on studies dealing with the linguistic approximation of such atypical fuzzy sets (Kowalczyk, 1998, 1999; Scott & Whalen, 2000; Whalen & Schott, 2001; Garibaldi & John, 2003; Garibaldi et al., 2004), we adopt here a simple qualitative approach to articulate the *if-then rules*. For linguistic modifiers or hedges, which are often used to express ambiguity or caution (Wenstop, 1976), our approach adheres to the following conventions:

(a) for non-convex sets, the lower and upper limit of the set is included in the rule with the connective 'to',

(b) for visually evident multimodal sets, the subnormal set is included in the rule using the hedge 'possibly'.

## Fuzzy type definition

Researchers have already applied fuzzy clustering techniques for defining groups within assemblages, yet we do not consider the potential of the method fairly highlighted. It is true that clustering results may not and most probably will not come close to results of material specialist. Before taking this as a fact though, we should ensure we have sufficiently added the information needed for the specific model to be made. We propose an iterative procedure where by means of visualization, we can reflect on how well or bad the conceptual model is reconstructed. Reflection can let us readjust the data, concepts and parameters we utilize in the digital model construction. In this section, we propose to estimate the number of morphological modes that exist in a pottery assemblage, locate them, and visualize an overview of the data and the results. The approach we propose can be parallelized with distance methods, principal components, and type variety in the taxonomic classification of arrangements of Dunnell (1971) and Banning (2020).

### Number of variants

Before we locate subgroups in the data, we first have to define the number of subgroups we should be looking for, denoted *k*. We define *k* following numerical information criteria and then visually inspecting the user interface described in section 'Network embedding'. The numerical information criteria we use are the following: elbow method, silhouette method, gap statistic, Calinsky criterion and affinity propagation (Kaufman & Rousseeuw, 2009; Tibshirani et al., 2001; Caliński & Harabasz, 1974; Frey & Dueck, 2007). Each metric is more or less well-known in the field of statistics and machine learning and each provide different optimization process, therefore it is not always straightforward to select one potential *k* number of subgroups, especially without taking more information into account. In a typological arrangement, the number of subgroups could be large if there is a large range in the analyzed data, but in the current case study, we rather select a small number of groups since these represent variants within a type, which is the most detailed categorization in SRSW typology. If we continue defining more sub-groups, clusters would be tighter but this would also fragment the original type and dissociate material specialists and classification practices. Additionally, the user interface allows to inspect the relationships between profiles, in micro and macro scale, and therefore aids with reflecting on whether the suggested number of groups is sensible. Given the selected number of clusters, we proceed with locating the variants, in the following section.

### Labelling of variants

Based on the number of variants detected, we employ fuzzy clustering to locate the *k* groups (J. C. Dunn, 1973; Bezdek, 2013; Lai Chung & Lee, 1994; Pal et al., 1996). The algorithm we use is fuzzy *k*-means, where *k* stands for the number of variants we wish to define and the algorithm takes as input the distance matrix representing (dis)similarity between profiles (see section 'Dissimilarity between profiles'). Fuzzy *k*-means creates *k* groups of profiles or clusters, where each profile belongs to all clusters with a certain support. Within each fuzzy cluster we identify:

- The most central sherds or typical cases, which are closer to the theoretical centrotype and therefore have high support in the crisp cluster they belong to.
- The most peripheral sherds or atypical cases, which fall in the boundaries of the cluster in the data space and therefore have the lowest support in the crisp cluster they belong to.
- Marginal cases, which have a small difference in the support value of the dominant crisp class and the second to dominant crisp class. It is noted that in this work, we consider the value of 0.01 for marginal case definition, however this is only a convention we adopt in this paper.

**Network embedding**

The dissimilarity matrix (see section 'Dissimilarity between profiles') can be considered as the weighted adjacency matrix of a fully connected network. The nodes of the network refer to the sherds and the links refer to the distances between sherds. Unnecessary links can be eliminated with the STAD algorithm proposed by Alcaide and Aerts (2020) to construct a network representation that has the links needed to present local and global relationships between data. Consequently, the original distance matrix is optimally transformed into a network visualization, where the nodes are the profiles included in the data and links are the connections retained by the STAD algorithm. The visualization is presented in the 2D screen as a result of the network embedding implementation. Alternative 2D representations have been used in the field of digital typological arrangement such as UMAP (McInnes et al., 2020) and t-SNE (Hinton & Roweis, 2002), which can perform well but they provide a point cloud and not a network representation.

### User Interface

To provide an overview of the data generated in section 'Fuzzy type definition' including the technical drawings and their metadata, and allow researchers to zoom in on more detail on demand, we employ a custom-made shinyApp (Kafetzaki, 2022b) using R shiny (Chang et al., 2020).

In the interface, the nodes of the network are associated with the technical drawing of the sherd or vessel and a processed version of the image is displayed as node. The nodes can be colored according to the set of filters we construct. The filters can be continuous or categorical variables and the color is applied according to the value of the variable with color brushing. Filters can be also applied to individual or group of nodes such that the selection is highlighted. Apart from the fuzzy clustering results, the nodes are also associated with the retrieved geometric morphology data (section 'Geometric morphology measures'), fuzzy polythetic descriptors section 'Fuzzy type description') and profile metadata derived from the archaeological contexts they were found.

The interactive visual overview summarizes much information derived from the digital (re)arrangement process and connects to the familiar representation of the technical drawing. The visualization spans the whole range of profiles provided and it has been used so far, for up to 500 profiles. The usage of the interface makes it easier to interpret the data, access insights they provide, generate hypotheses, and help work towards providing answers to our research questions. This is why we consider our visualisation approach an essential part of the digital model and further improving the user interface is part of our future work.

## Shape quantification

### Background information

Shape analysis methodologies (Pavlidis, 1978; Mingqiang et al., 2008; Li et al., 2018) provide the means to trace morphological features. These methods have been applied to a wide range of archaeological finds, such as lithics, stone tools and axes, skeletal remains and cranial bases, and architectural elements (Leese & Main, 1983; Gero & Mazzullo, 1984; Rovner, 1995; Lestrel et al., 2004; Lenardi & Merwin, 2010; Cardillo, 2010; Carlo et al., 2011; Lo Buglio et al., 2013; Caple, 2017; Hoggard et al., 2019). Quantitatively measuring pottery form is not new to archaeological practice either. One of the earliest and most intuitive methods involves recording ratios of geometric measures from vessels (Webster, 1964; Hardy-Smith, 1974). More systematic techniques tailored to vessel morphology quantification have been also developed. Taking into account the whole vessel, the mosaic method (J. D. Wilcock, 1974; J. Wilcock & Shennan, 1975) uses a sequence of hierarchical profile area codes. Considering the outer profile line, the sliced method (J. D. Wilcock, 1974; J. Wilcock & Shennan, 1975) produces a vector of radii to height ratios from vessel's midline, while the swept radii method (Liming et al., 1989) produces a similar vector using as reference point half of a vessel's height measured in the midline. Using the profile tangent as a means to quantify and store pottery form has been discussed by Main (1987) while the one dimensional vector encodings are extended to the Cartesian, polar, tangent and curvature representations (Saragusti et al., 2005; Gilboa et al., 2004; Karasik et al., 2005; Smith et al., 2014). From the shape transform domain, Fourier analysis is applied to analyze pottery form (Saragusti et al., 2005; Wang & Marwick, 2020). Mathematical morphology methods have been also implemented to retrieve pottery form data. In a comparable approach, Martínez-Carrillo et al. (2010) used a scale-space method to compare pottery. They set three anchor points to complete profiles and allowed similarity computation of fragments and complete profiles if at least one anchor point is available. Lucena et al. (2016) quantified pottery images using four characteristic curves: dilation, erosion, opening, and closing. They then computed pairwise Euclidean distance. By splitting the profile into lip, neck, body, base and handle they facilitated the comparison of both complete and incomplete profiles. Another mathematical morphology application is reported by Lucena et al. (2017) where each profile was represented with a node chain and similarity was computed using pairwise energy of deformation. Finally, neural networks have been utilized for pottery morphological analysis. Such an approach (Parisotto et al., 2022), quantifies form through the non-linear features learned in the latent representation space of a stacked sparse autoencoder (SSAE) network.

Evidently, there are several ways to quantify shape information. Some methods quantify most of the total amount of information in the form while other methods quantify specific aspects of the form. In this paper, shape quantification is the primary part of the analysis pipeline. However, our aim is not to provide a detailed review of pottery form quantification. The choice of the shape quantification depends on the research question and the material at hand. Hence we propose three approaches to quantify the pottery form in subsections 'One-dimensional outline transformation', 'One-dimensional profile transformation', and 'Geometric morphology measures'. The first two techniques preserve most shape information in the profiles while the last quantifies specific profile features.

## Image data processing

In total, 601 image files of technical drawings in jpeg format and 300 dpi are used in the analysis presented in this paper. The size of the files is varying depending on the profile itself, for instance a simple and incomplete profile is 16 KB while a large complete profile with decoration is 337 KB. Each technical drawing contains the vessel or sherd profile and the scale. We use R in RStudio (R Core Team, 2020; RStudio Team, 2016) as our main software for data processing and for all consecutive analysis.

First, we define the rim height, $h$, for each of the profiles in the database, using a custom shiny app. Using this shiny app, we also specify whether the image contains a boundary. If it contains a boundary, we specify as *TRUE* the value of the Boolean used to control the cropping, for each of the profiles in the database. The image is imported in RGB format in R and is cropped accordingly. Then, since the image may contain grey values, a global threshold of value 0.9 is applied to retrieve a binary (black and white) matrix. Thereupon, we automatically calculate the bounding box of the profile and the bounding box of the scale. The image is cropped again, automatically, such that it contains only the profile, while the scale information is stored and the rest of the image is discarded. The retrieved profile is a binary matrix $S_{\mathrm{X}\times\mathrm{Y}}$, where X is the profile width and Y the profile height.

## One-dimensional outline transformation

The one-dimensional outline transformation (1D outline), quantifies the outline retrieved by the profile, unfolds and saves the new data in a vector $O_L$ , where $O$ is the transformed outline value for its length $L$. This is a contour-based method inspired by the Cartesian representation method discussed by Saragusti et al. (2005) and it can be applied to any set of profiles as long as the profile segments can be coherently compared.

Technically, based on the height of the segment that is already provided as input, the width of the rim profile $W$ is automatically calculated for each profile and the profile binary matrix $S_{\mathrm{X}\times\mathrm{Y}}$ is cropped accordingly to $M_{\mathrm{W}\times\mathrm{H}}$. The cropped profile matrix is further used to retrieve the one-dimensional outline.

Each $M_{\mathrm{W}\times\mathrm{H}}$ is scaled to $M'_{\mathrm{W}\times\mathrm{H}}$ using a scale factor $s$, which is a numeric scalar estimated for each profile. The scale factor is specified such that the length of the periphery is equal to the predefined global value $L$, while the original aspect ratio of each rim is maintained. We position $M'_{\mathrm{W}\times\mathrm{H}}$ on a plane by considering the indices of the matrix entries as Cartesian coordinates. We then retrieve a one-dimensional Cartesian representation of the profile periphery, $p_L$, by taking the outer, top and inner projections of the matrix. In contrast to the original suggestion by Saragusti et al. (2005) where the origin is the vessel's axis of cylindrical symmetry, here we choose the origin or reference point to be the origin of the Cartesian axis, which makes our approach applicable to profiles for which the diameter of the vessel is unknown.

Using this approach, the two-dimensional profile segment is essentially unfolded to a one-dimensional vector, as illustrated in ***Fig. 3***. Starting from the sherd's outline bottom outer point, $A = (x_1, y_1)$, $x_1$ is saved and $y_1$ is discarded. Following the outline until the bottom inner point $E = (x_l, y_l)$, each $x_i$ with $i \in \{1, L\}$ is saved in a vector $p_L = (x_1, x_2, \ldots, x_l)$. Then, we normalize the vector by setting the first highest point of the outline (e.g. point C in ***Fig. 3***) to zero. Therefore, point C corresponds to the most outer point of the rim top and the one after the last point of the outer part of the outline, $O_{outer}$. Point C together with every consecutive point in the same height correspond to the flat top of the outline, $O_{top}$, while all the rest of the points constitute $O_{inner}$, the outline segment of the inner part of the rim profile. For visually distinguishing better the different segments of the outline, as well as the reference point C and all points belonging in flat top, $O_{top}$ can be set to zero on the unfolded vector. Under this representation, the original distance of the points on the x-axis is preserved and the two-dimensional rim shape can be reconstructed using this representation, as long as the profile has no hollows.

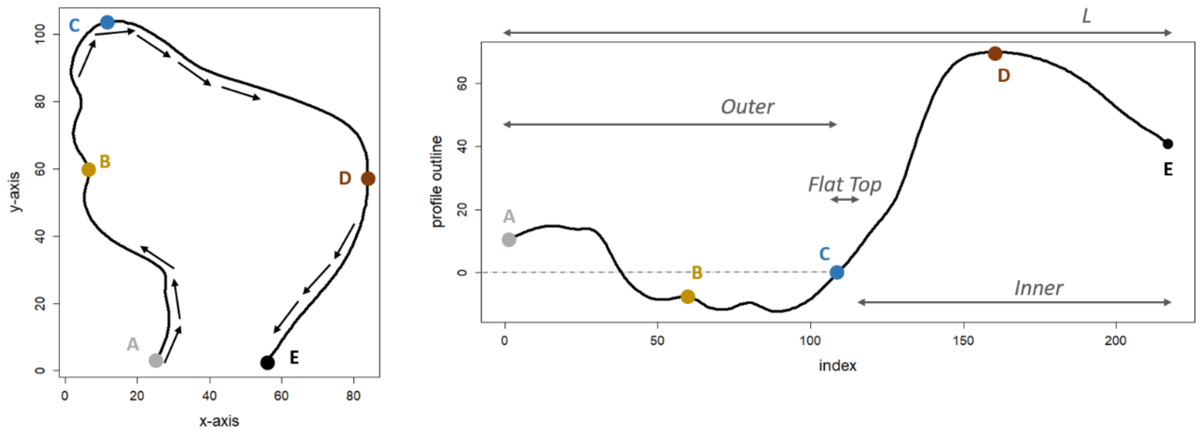


***Fig. 3*** *Example on the retrieval of the one-dimensional outline: (left) outline of a rim profile on the Cartesian coordinate plane, (right) unfolded outline of length L, following our methodology*

When certain hollows are present in the rim outline, such as one due to an undercut rim, only the information regarding the location and the width of the hollow is preserved in the representation we propose here. To retain the complete information of the hollow, a second vector referring only to the hollow should be produced to capture its full shape. In this paper, we use this shape quantification method to analyze profiles with rim segments from types SRSW 1B150 (section 'The case of SRSW 1B150') and equal-height segments of type 1A130 (section 'The case of SRSW 1A130'), which have no hollows.

## One-dimensional profile transformation

The one-dimensional profile transformation (1D profile) quantifies the wall of the profile using a Generalized Additive Model (GAM) (Hastie & Tibshirani, 1986) and saves the new data in a vector $GAM_L$ where $GAM$ is the transformed profile value for its length $L$. This method is also applicable to any set of profiles as long as the profile segments can be coherently compared and in this paper, we choose to apply this method to complete profiles.

Starting from the binary matrix $S_{X \times Y}$, the values representing the wall associated with the base of the profile are erased. This is automatically implemented by locating the bottom inner point of the profile wall plus a margin (here 5 pixels) and replacing the black values that cluster together at the bottom with white values.

Consecutively, the binary matrix is resized such that the height is equal to the predefined global value $L$ and the original aspect ratio is maintained. Next, the GAM is computed for each profile using 107 equally-spaced knots and generalized cross-validation to compute the smoothing parameter. Finally, the retrieved vector is normalized using min-max normalization such that the top and the bottom can be used as reference points in a relative comparison of the form for the set of profiles.

## Geometric morphology measures

Measurement-based quantification is an information non-preserving technique, since it does not allow an exhaustive reconstruction solely from the derived data. However, the measures are *essential parameters* (Kurnianggoro et al., 2018) and focus mostly on what the material specialist perceives as important. As such, defining the most essential shape-related variables as point measures creates an advantage for the interpretation and further analysis. Specifically, the measures serve as input for the algorithms used in this paper to attach a fuzzy polythetic descriptor and to emphasize aspects of the form in the fuzzy arrangement.

The measures proposed in the original typological model are now automatically derived from the images. In addition to these primary measures included in the SRSW typological model, we calculate derived measures that capture more of the complexity of the shape. Part of the measures are taken from Neal and Russ (2012) and from Kurnianggoro et al. (2018) while other measures are introduced here, specifically for the material under study. Below we list all geometric measures that are used in our analysis. Scale is automatically retrieved and used to transform the data in original dimension.

Global measures referring to the profile matrix $S_{\mathrm{X} \times \mathrm{Y}}$ defined in the Cartesian coordinate system:

i. Is full profile (Boolean). TRUE if both base-line and rim-line are present in the technical drawing.
ii. Profile height $Y$
iii. Rim diameter $RD = S_{[x_{max},\ Y]} - S_{[x_{min},\ Y]}$, where $x_{max}$ is $\max(x_i)$ for $i \in [1,..,\mathrm{X}]$ and $x_{min}$ is $\min(x_i)$ for $i \in [1,..,\mathrm{H}]$
iv. Base diameter $BD = S_{[x_{max},\ 1]} - S_{[x_{min},\ 1]}$
v. Height Width ratio $HW = \frac{Y}{RD}$
vi. Wall thickness at 2/3 of Height $WT_{2/3} = S_{\left[x_{max},\ \frac{2Y}{3}\right]} - S_{\left[x_{min},\ \frac{2Y}{3}\right]}$
vii. Wall inclination $WI = -(1 + WI_{sin})$ for $WI_{sin} < 0$ and $WI = 1 - WI_{sin}$ for $WI_{sin} > 0$, where $WI_{sin} = \sin\left(\frac{Y}{\sqrt{(S_{[x_{min},\ Y]} - S_{[x_{min},\ 1]})^2}}\right)$
viii. Inclination below the rim $RIB = -(1 + RIB_{sin})$ for $RIB_{sin} < 0$ and $RIB = 1 - RIB_{sin}$ for $RIB_{sin} > 0$, where $RIB_{sin} = \sin\left(\frac{H}{\sqrt{(S_{[x_{min}+z,\ H]} - S_{[x_{min}+z,\ 2H]})^2}}\right)$, for $z = \left\{0,\ \frac{WT}{2}, WT\right\}$ and $H$ is the rim height (see following list).
ix. Position of the lines drawn in the inner and the outer profile with respect to the profile height. These can be part of a groove or decoration.

Rim measures referring to the rim profile matrix $M_{\mathrm{W} \times \mathrm{H}}$, extracted from the profile matrix $S_{\mathrm{X} \times \mathrm{Y}}$:

i. Rim height, calculated using the shiny app $H$
ii. Outer difference length $DL_{outer} = O_{outer}[1] - O_{outer}[H]$
iii. Inner difference length $DL_{inner} = O_{inner}[1] - O_{inner}[H]$
iv. Outer protuberance length is max(protuberance using the most outer point , protuberance using the thickest point) $PL_{outer} = max(\frac{2 \times Area_{outer}}{Base_{outer}}, \frac{2 \times Area_{maxWTout}}{Base_{maxWTout}})$
v. Inner protuberance length is max(protuberance using the most inner point , protuberance using the thickest point) $PL_{inner} = max(\frac{2 \times Area_{inner}}{Base_{inner}}, \frac{2 \times Area_{maxWTinn}}{Base_{maxWTinn}})$
vi. Rim width $RW = \min(O_{outer}\ [i]) - \max(O_{inner}\ [i])$ where I ∈ 1, .., H
vii. Rim thickness $RT = O_{inner} - O_{outer}$ and summary statistics measures of RT, where $i \in [1,..,\mathrm{H}]$:
   - $RT_{max} = \max(RT[i])$
   - $RT_{min} = \min(RT[i])$
   - $RT_{avg} = \frac{\sum_{i=1}^{H} RT[i]}{H}$
   - $RT_{sd} = \sqrt{\frac{\sum_{i=1}^{H}(RT[i] - R_{avg})^2}{H-1}}$
   - $RT_{median} = RT'\left[\frac{H+1}{2}\right]$ if $H$ is odd and $RT_{median} = \frac{1}{2}\left(RT'\left[\frac{H}{2}+1\right] + RT'\left[\frac{H}{2}\right]\right)$ if $H$ is even, where $RT'$ is the sorted $RT$.

viii. Elongation, for maximum, minimum and average rim thickness: $El_{max} = \frac{H}{RT_{max}}$, $El_{min} = \frac{H}{RT_{min}}$, $El_{avg} = \frac{H}{RT_{avg}}$

ix. Ratio of rim top thickness over bottom rim thickness $TB = \frac{|O_{top}|}{O_{inner}[1] - O_{outer}[1]}$.

x. Ratio of rim top thickness over maximum rim thickness $TM = \frac{O_{inner}[H] - O_{outer}[H]}{RT_{max}}$.

xi. Eccentricity $Ec = \sqrt{1 - \frac{minoraxis^2}{majoraxis^2}}$, calculated using the function 'computeFeatures' in Rpackage 'EBImage' (Pau et al., 2010).

xii. Radis ratio $RR = \frac{radius_{min}}{radius_{max}}$, where $radius_{max}$ and $radius_{min}$ are calculated using the function 'computeFeatures' in Rpackage 'EBImage' (Pau et al., 2010).

xiii. Aspect ratio $AR = \frac{2radius_{max}}{2radius_{min}}$

xiv. Roundness $R = \frac{4RimArea}{\pi(2radius_{max})^2}$

xv. Form factor $FF = \frac{4\pi RimArea}{|RimPerimeter|^2}$

xvi. Curl $CR = \frac{|RimPerimeter|}{H}$

xvii. Extent-1 $E1 = \frac{RimArea}{RimBoundingBoxArea}$

xviii. Block% $B\% = 1 - \frac{RimBoundingBoxArea - RimArea}{RimBoundingBoxArea}$

xix. Trapezoid% $T\% = 1 - \frac{RimTrapezoidArea - RimArea}{RimTrapezoidArea}$

xx. Log rim irregularity with respect to maximum elongation $I_{WT} = \log(\frac{|RimPerimeter\ (excl.Base)|}{El_{max}})$

# Dissimilarity between profiles

A necessary step towards grouping arrangement with algorithmic fuzzy type varieties is to compute the (dis)similarities between profiles. A shape quantification transformation, as presented in section 'Shape quantification', should be in place to proceed with (dis)similarity computation. Although the shape quantification should be considered on a case-by-case basis, the (dis)similarity between profiles is quantified following the automatic approach presented in this section. The goal of the process is to end up with the distance matrix that produces the most informative view while maintaining local and global relationships between profiles.

## Distance computation

This section accommodates possible ways to compute pairwise (dis)similarity. Several metrics could be applicable in this setting, but it is out of the scope of this paper to provide a full review for each quantification. We use five distance functions that take the order of the data into account: Minkowski with $p = 4$, Euclidean, Manhattan, Chebyshev, and Canberra. The functions are applied to the one-dimensional vector resulting from shape transformation. This vector refers either to the 1D outline, 1D profile or a set of geometric measures, for the length of the vector $L$.

Minkowski is a function that accommodates the parameter $p$, where $p = 1$ corresponds to the Manhattan distance and $p = 2$ to the Euclidean distance while it approximates the Chebyshev when $\lim_{p \to \infty} p$. In this paper, we use $p = 4$ in the Minkowski function $d(A, \mathrm{B}) = \sqrt[p]{\sum_{i=1}^{L} (A_i - B_i)^{\mathrm{p}}}$ to compute the Minkowski distance between profiles A and B for the length $L$ of the shape vector. For clarity, we provide the functions for Euclidean, Manhattan and Chebyshev distance functions: Euclidean distance between profiles A and B is $d(A, \mathrm{B}) = \sqrt{\sum_{i=1}^{L} (A_i - B_i)^2}$. Manhattan is $d(A, \mathrm{B}) = \sum_{i=1}^{L} |A_i - B_i|$, and Chebyshev is $d(A, \mathrm{B}) = \max(\sum_{i=1}^{L} |A_i - B_i|)$. Finally, Canberra is $d(A, \mathrm{B}) = \sum_{i=1}^{L} \frac{|A_i - B_i|}{|A_i| + |B_i|}$, between profiles A and B, for the length $L$ of the shape vector. The smaller the pairwise distance value, computed under one of the metrics, the closer the profiles are in the quantified shape space, with identical profiles having a distance value equal to zero.

## Distance consolidation

There could be cases where we have arguments to include information derived from different shape quantification approaches. Such cases arise when we aim to merge two or more distance matrices produced by one shape quantification method or when we aim to merge at least one distance matrix and at least one geometric measure. Consolidation of different shape quantification approaches is optional, but when performed, the way to proceed consists of two steps.

The first step is to perform Principal Component Analysis (PCA) (Pearson, 1901) such that we change the basis of the data. Each distance matrix is transformed using singular value decomposition and the first few principal components are retained. The number of chosen components is determined based on cumulative variance explained heuristics. First, using a scree plot we inspect where the variance gained by retaining additional eigenvalues is relatively small. Second, we control our choice such that we select the smallest number of eigenvalues that returns equal or larger than 95% cumulative variance explained. The result is the transformed (scores) data of dimension $N \times V$ where $N$ is the number of profiles present in the original data and $V$ is the number of eigenvalues retained.

The second step of the consolidation is a join of the transformed data, having the profiles ID as the join key, meaning that the data are combined side by side. In case we aim to include entirely the information provided by a geometric measure in the consolidated data, the first step is skipped, and we simply join the transformed data with the measures using the profiles ID as the join key. As a result, we have a data of dimension $N \times V'$ where $V'$ is equal to the sum of the number of eigenvalues retained for each data matrix and the number of measures we wish to include. The consolidated data is used to compute the dissimilarity between the profiles following the procedure discussed in the previous subsection ('Distance computation').

## Distance selection

Both when the shape quantification data is consolidated and when not, we perform distance metric selection after distance computation. The choice of the distance metric is important since we require this metric to represent pairwise dissimilarity in a global and local level. The process of selection is automatically performed in R using custom-made scripts (Kafetzaki, 2023). The aptness of the distance metric in quantifying the profile similarity is evaluated against three representations and seven criteria.

The first representation is the STAD reconstruction (see section 'Network embedding'), from which we derive (1) the number of graph edges and (2) the STAD correlation from the built-in functions. We include the number of edges as a criterion because we aim to keep only the necessary links to reconstruct the map of the type which should be useful in imprinting relations between profiles and network substructures made because of the relationships.

The second representation is the Shepard diagram (De Leeuw & Mair, 2015) by means of which we can check the error of projecting high-dimensional data in two dimensions and compute (3) the Shepard Adjusted R-squared (Adj-$R^2$). The original distances, resulting from each distance metric, are compared to the distances provided by the network embedded in the 2D space of the computer screen. A regression line is fit and the Adj-$R^2$ of the fitted line provides numerical information on the quality of the reconstruction. By construction Adj-$R^2 \in [0, 1]$ and the optimal value is 1 occurring when the distances in the 2D reconstruction are exactly the same with the distances in the high-dimensional space.

The third representation is the STAD's adjacency matrix reconstruction based on the Dijkstra's shortest path algorithm (Dijkstra, 1959). Dijkstra's reconstruction is compared to the original distance matrix computed for each distance metric and the following criteria are computed: (4) Median absolute difference, (5) IQR of absolute difference, (6) Standard deviation of absolute difference, and (7) MAD of absolute difference.

To evaluate the seven criteria, we carry out a simulation that performs STAD reconstruction under different seeds and we tabulate the value of each criterion, for each run, and for each distance metric. We perform 100 simulations therefore we end up with a table of dimensions $7 \times 100 \times 5$. To select the distance metric that best satisfies the expectations on the mapping, we compute the average of each distance metric for each criterion, then the distance metric with the minimum loss is ranked first. We check for ties in the rank using the process described in section 'Statistical difference between group means'. The distance metric that is ranked first the most over all seven criteria is selected.

## Statistical difference between group means

For a numeric variable, the differences in the average values in two or more groups can be statistically tested for significance. This possibility is interesting in our setting, first, for inferring ties in the distance selection process described above and second, for testing the difference in geometric measures between the algorithmically proposed number of classes in the results section.

The analysis is performed using one-way ANOVA (Chambers et al., 1992) and post-hoc Tukey procedure (Yandell, 2017) to simultaneously infer whether the means of the groups are significantly different. The results are valid as long as the residuals are normal based on the Shapiro test (Royston, 1982a, 1982b) and homoscedastic based on Levene's test (Fox, 2015; Fox & Weisberg, 2018). If the residual analysis shows departures from the assumed model, we perform the non-parametric Kruskal-Wallis rank sum test (Hollander et al., 2013) and the Dunn's test as post-hoc (O. J. Dunn, 1964).

# Results

## Fuzzy rim description

As already highlighted, polythetic descriptors are an important part of the typological model presented here. In this section, we provide a fuzzy dimension of recurrent polythetic SRSW rim descriptors. To specify the membership functions in this section, first, we assume they can be mathematically described by a Gaussian or a Logistic function, second, that the shape of the input and the output membership functions in each rule is the same, third, that we have a dominant rule for every value in the input space, and fourth, that the completeness level is between 0.25 to 0.5 as suggested by Bouchon-Meunier et al. (1996). Considering that the geometric measures are designed such that each quantifies a specific morphological property of the rim profile, it is straightforward to select the geometric measures that are associated with each fuzzy descriptor. For the antecedents containing two fuzzy sets, we use a monotonically decreasing and a monotonically increasing function where one is the complement of the other. Taking the above into account, we specify the input membership functions, visually summarized in ***Fig. 4***.

The most evident membership functions in this section are the ones referring to the descriptors 'rounded', 'horizontally flattened' and 'vertically flattened' which are also similar in design. Since the input measures are defined in [0,1] where 0 corresponds to 'not at all' and 1 corresponds to 'completely', it follows that the inflection point should be at 0.5. At the same time, the degree of truth becomes higher for values deviating from the inflection point and approaches the peak before the input approaches the boundaries. Specifically, we set the degree of truth larger than 0.95 for values smaller than 0.3 and larger than 0.7. As a result, we define the fuzzy sets 'high' and 'low' for every $x$ denoting each input geometric measure involved in the rules as: $\mu_{high}(x; 12, 0.5) = \frac{1}{1+\exp(-12(x-0.5))}$, $\mu_{low}(x; -12, 0.5) = \frac{1}{1+\exp(-(-12)(x-0.5))}$. The fuzzy sets are plotted in ***Fig. 4*** (middle).

To define 'everted', we also define 'straight' and 'inverted'. The rims that are completely 'straight' should have values equal to zero for the geometric measures involved in the rules. Around zero, we allow a standard deviation of five pixels, which is 0.084 cm, therefore the input function becomes $\mu_{zero}(x; 0, 0.084) = \exp\left(-\frac{(x-0)^2}{2(0.084)^2}\right)$. For the positive and negative functions, we set $x_0$ equal to 10 pixels, therefore $x_0 = 0.168\ cm$ and to meet the assumption of the minimum completeness level we define $\mu_{negative}(x; -17.9, -0.168) = \frac{1}{1+\exp(-(-17.9)(x-(-0.168)))}$, $\mu_{positive}(x; 17.9, 0.168) = \frac{1}{1+\exp(-17.9(x-0.168))}$ and the inflection points are therefore calculated at -1.3 mm and 1.3 mm. The fuzzy sets for *zero*, *positive* and *negative* are plotted in ***Fig. 4*** (left).

Finally, to define 'thickened', we also define 'plain' and 'thinned'. A totally plain rim would have a ratio of median wall thickness and bottom wall thickness of 1. Around 1 we allow a standard deviation of 0.15, therefore the input function becomes $\mu_{medium}(x; 1, 0.15) = \exp\left(-\frac{(x-1)^2}{2(0.15)^2}\right)$. For the positive and negative sets we consider a rim thickened with *support* 0.5 when the median wall thickness is 20% larger than the bottom wall thickness, therefore the membership functions are $\mu_{high}(x; 10, 0.2) = \frac{1}{1+\exp(-10(x-0.2))}$, $\mu_{low}(x; -10, 0.2) = \frac{1}{1+\exp(-(-10)(x-0.2))}$ and the corresponding sets are plotted in ***Fig. 4*** (right).

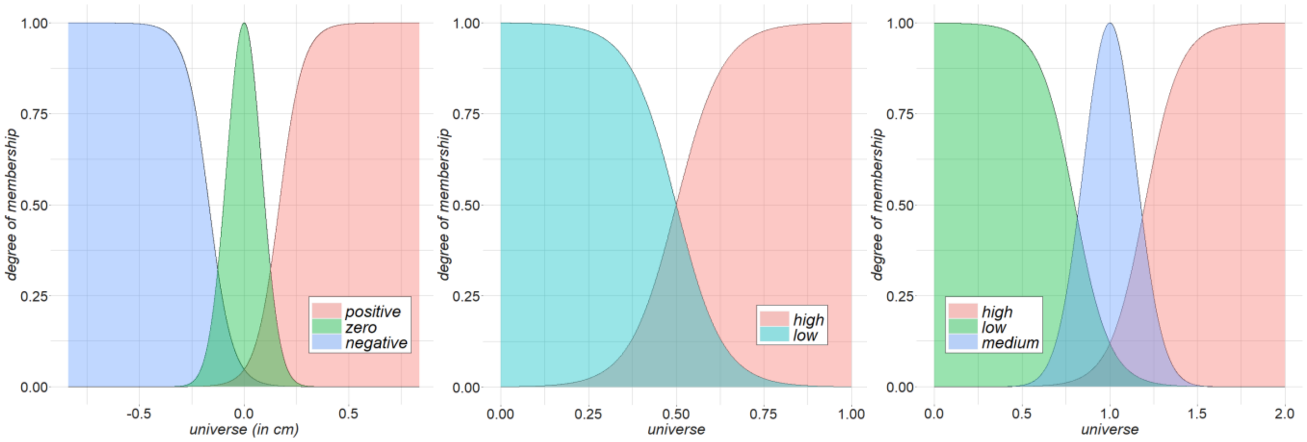


***Fig. 4*** *Input membership functions for polythetic rim descriptors: (left) inverted – straight – everted, (middle) in the following three systems: horizontally flattened, vertically flattened, and rounded, (right) thickened – plain – thinned.*

Next, we demonstrate the rules that are used to build each fuzzy set.

**Rim is inverted, straight, everted**

Fuzzy set-1 contains the descriptors {inverted, straight, everted} and is defined by the two geometric measures that capture the difference in length between the rim top and bottom outline. The following rules are constructed:

Rule 1.1: *If* (the outer difference is negative) *and* (the inner difference is negative) *then* the rim is inverted.

Rule 1.2: *If* (the outer difference is zero) *and* (the inner difference is zero) *then* the rim is straight.

Rule 1.3: *If* (the outer difference is positive) *and* (the inner difference is positive) *then* the rim is everted.

The result is the fuzzy set $\widetilde{Set_1} = \left\{\frac{support_{inverted}}{inverted} + \frac{support_{straight}}{straight} + \frac{support_{everted}}{everted}\right\}$.

**Rim is horizontally flattened**

Fuzzy set-2 contains the descriptors {horizontally flattened, not horizontally flattened} and is defined by the geometric measures of rim top thickness/rim bottom thickness and rim top thickness/maximum rim thickness The following rules are constructed:

Rule 2.1: *If* (the ratio of rim top thickness over bottom rim thickness is high) *and* (the ratio of rim top thickness over maximum rim thickness is high) *then* (the rim is horizontally flattened).

Rule 2.2: *If* (the ratio of rim top thickness over bottom rim thickness is low) *and* (the ratio of rim top thickness over maximum rim thickness is low) *then* (the rim is not horizontally flattened).

The result is $\widetilde{Set_2} = \left\{\frac{support_{horizontally\ flattened}}{horizontally\ flattened} + \frac{support_{not\ horizontally\ flattened}}{not\ horizontally\ flattened}\right\}$.

**Rim is vertically flattened at the exterior or the interior**

Fuzzy set-3 contains the descriptors {vertically flattened, not vertically flattened} and is defined by the geometric measures of vertical sequence length and the rim height. The flattening refers to outline section forming 90 degrees angle with the rim diameter conceivable straight. Fuzzy set-3 is constructed in a similar way for both exterior and interior descriptors, and the vertical sequence length refers either to the exterior and to the interior, with respect to the attributed descriptor. The following rules are constructed:

Rule 3.1: *If* (the ratio of the vertical sequence length and the height is high) *then* (the rim is vertically flattened).

Rule 3.2: *If* (the ratio of the vertical sequence length and the height is low) *then* (the rim is not vertically flattened).

The result is $\widetilde{Set_3} = \left\{\frac{support_{vertically\ flattened}}{vertically\ flattened} + \frac{support_{not\ vertically\ flattened}}{not\ vertically\ flattened}\right\}$.

**Rim is rounded**

Fuzzy set-4 contains the descriptors {rounded, not rounded} and is defined by the geometric measures of roundness and eccentricity. The following rules are constructed:

Rule 4.1: *If* (the roundness is high) *or* (the eccentricity is low) *then* (the rim is rounded).

Rule 4.2: *If* (the roundness is low) *or* (the eccentricity is high) *then* (the rim is not rounded).

The result is $\widetilde{Set_4} = \left\{\frac{support_{rounded}}{rounded} + \frac{support_{not\ rounded}}{not\ rounded}\right\}$.

**Rim is thickened, plain, thinned**

Fuzzy set-5 contains the descriptors {thickened, plain, thinned} and is defined by the geometric measures of rim thickness, specifically the overall median of the rim thickness and thickness measured at the bottom of the rim. The following rules are constructed:

Rule 5.1: *If* (the ratio of the median wall thickness and the rim bottom thickness is high) *then* (the rim is thickened).

Rule 5.2: *If* (the ratio of the median wall thickness and the rim bottom thickness is medium) *then* (the rim is plain).

Rule 5.3: *If* (the ratio of the median wall thickness and the rim bottom thickness is low) *then* (the rim is thinned).

The result is $\widetilde{Set_5} = \left\{\frac{support_{thickened}}{thickened} + \frac{support_{plain}}{plain} + \frac{support_{thinned}}{thinned}\right\}$.

## Fuzzy functional interpretation based on global shape

In this section, we study the global morphology of complete profiles and we propose a working model that associates the global vessel morphology with pre-established SRSW labels in the original typological model (Poblome, 1999). Our aim is to provide a fuzzy dimension to the functional class labels and rather not to claim that functional interpretation can be conducted based on our model.

The definition of the membership functions differs from the approach outlined in the section 'Fuzzy rim description', since we make use of the crisp label provided by the material specialist for each profile. We implement fuzzy logic to illustrate how the measurable aspects of the profile can be used to attribute fuzzy functional group (FG) labels within the five functional groups defined in the original typological model.

To measure the global shape we focus on the complete profiles, since incomplete profiles would introduce missing information in the retrieved data. From the global geometric measures presented in section 'Shape quantification', we work with the following six: rim diameter, base diameter, profile inclination, height/width ratio, height, and wall thickness measured at 2/3 of the profile height. A total of 288 complete profiles are analyzed in this section coming from 59 SRSW types-variants.

Following the process discussed in section 'Label-driven fuzzy sets', the membership functions are specified in parallel with the empirical probability density functions for the selected six global measures (see ***Fig. 5***). The sample size is not balanced per FG, and although the number of observations in cups and plates (23) may be sufficient to calculate the empirical distributions, the number of complete containers are limited (7). However, this is not caused by a general lack of containers in Sagalassos, since the incomplete containers are not limited in number, but because containers are rather fragile due to the ratio of the size and wall thickness. In general, complete profiles are hard to come in proportion to the total amount of sherds retrieved at Sagalassos because of the taphonomy of the archaeological deposits, which are nearly never primary closed contexts, but mostly secondary or worse in nature, such as terracing fills or gradual abandonment contexts. That type of contexts imply a heavy life for pots and mostly sherds, in which they get to be reshuffled on more than one occasion, resulting in accumulated breakage. Considering archaeological reality, we include the containers in the analysis, although interpretations should be treated with care.

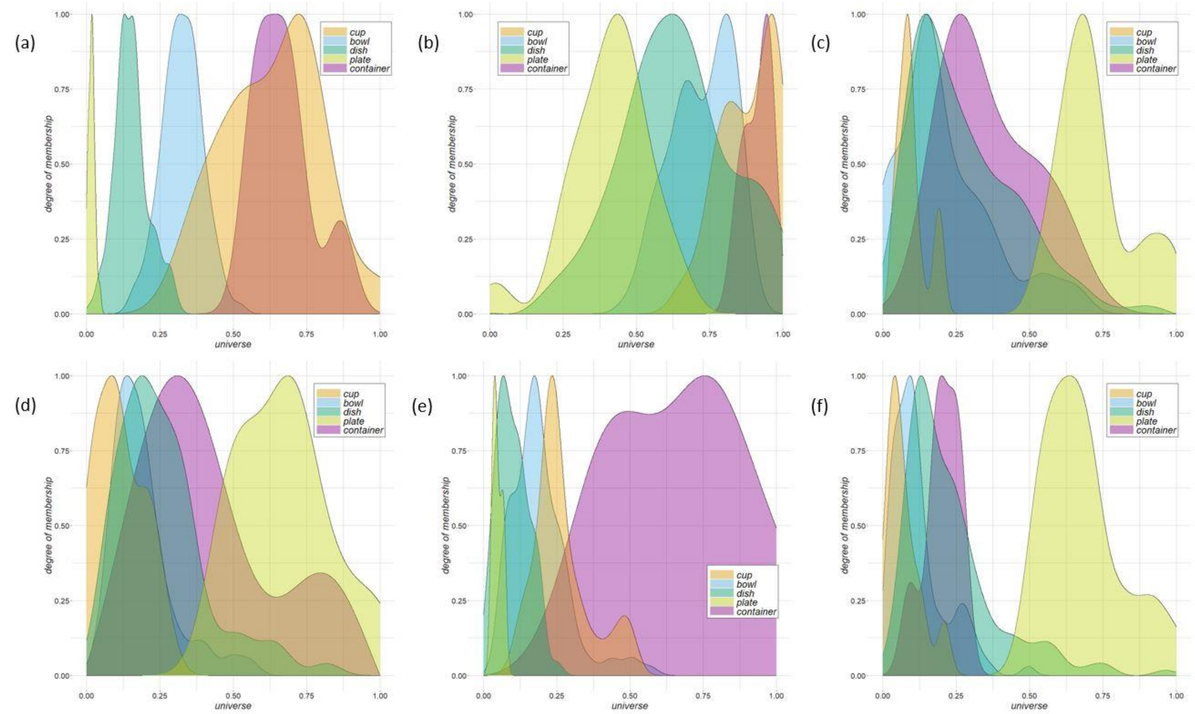


***Fig. 5*** *Membership functions in the functionality FIS. The variables used are: (a) Height/Width (b) Inclination (c) Rim diameter (d) Wall Thickness at 2/3 of Height (e) Height (f) Base diameter*

By observing the empirical distributions in ***Fig. 5***, it is evident that it would not be straightforward to articulate the if-then rules The number of geometric measures and the number of FG labels included in the rules already make it challenging, however, it is mainly the shape and overlap of the empirical distributions that impedes the creation of an eloquent rule. Using hedges and conventions discussed in section 'Label-driven fuzzy sets', the resulting *if-then* rules are the following:

Rule 6.1: *If* (height/width is moderate to high) *and* (inclination is possibly rather high or high) *and* (rim diameter is very small or possibly small) *and* (wall thickness at 2/3 is very small to possibly small) *and* (height is small or possibly moderate) *and* (base diameter is very small or possibly somewhat small) *then* (form resembles cup).

Rule 6.2: *If* (height/width is rather moderate) *and* (inclination is possibly larger than moderate to rather high) *and* (rim diameter is rather small or possibly moderate) *and* (wall thickness at 2/3 is rather small) *and* (height is small) *and* (base diameter is rather small or possibly small) *then* (form resembles bowl).

Rule 6.3: *If* (height/width is rather small) *and* (inclination is larger than moderate) *and* (rim diameter is rather small to moderate) *and* (wall thickness at 2/3 is small) *and* (height is very small to rather small) *and* (base diameter is rather small to small or possibly moderate) *then* (form resembles dish).

Rule 6.4: *If* (height/width is very small) *and* (inclination is possibly very small to rather moderate) *and* (rim diameter is rather large to possibly large) *and* (wall thickness at 2/3 is moderate to rather large) *and* (height is very small) *and* (base diameter is larger than moderate to possibly large) *then* (form resembles plate).

Rule 6.5: *If* (height/width is larger than moderate to possibly high) *and* (inclination is possibly rather high to high) *and* (rim diameter is small to larger than moderate) *and* (wall thickness at 2/3 is larger than small to possibly larger than large) *and* (height is possibly moderate to large) *and* (base diameter is rather small) *then* (form resembles container).

The output fuzzy set is the following:

$$\widetilde{Set_{FG}} = \left\{\frac{support_{cup}}{cup} + \frac{support_{bowl}}{bowl} + \frac{support_{dish}}{dish} + \frac{support_{plate}}{plate} + \frac{support_{container}}{container}\right\},$$

which means that each profile retains all labels with an algorithmically computed support. The maximally possible support is 1, but within the current design, to achieve a value of 1 would require all inputs to fall at the peak of the specified membership functions.

The proposed transformation inherently provides information on typical, atypical and marginal cases per FG. Considering the highest support as an indication for the most typical example of each functional group, in ***Table 1*** such cases are displayed. The most typical profile included in the data is the closest available example to the theoretical centrotype. The technical drawing of the most typical profile can be used as a reference point for material specialists on the combination of global morphological characteristics that make a profile resemble a particular functional group.

***Table 1*** *Output fuzzy set for the profiles with the highest support per functional class. The crisp result coincides with the expert's label*

| ID | Profile | Class | Fuzzy FG set |
|---|---|---|---|
| SADR021259 | 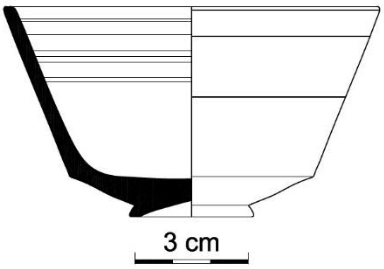  | Cup | $\left\{\frac{0.71}{cup}+\frac{0.01}{bowl}+\frac{0}{dish}+\frac{0}{plate}+\frac{0.03}{container}\right\}$ |
| SADR010878 | 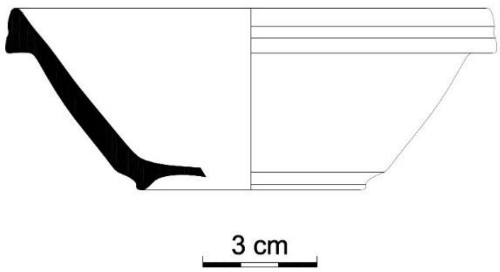  | Bowl | $\left\{\frac{0.08}{cup}+\frac{0.87}{bowl}+\frac{0}{dish}+\frac{0}{plate}+\frac{0}{container}\right\}$ |
| SADR010603 | 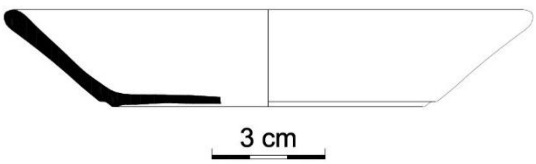  | Dish | $\left\{\frac{0.01}{cup}+\frac{0.10}{bowl}+\frac{0.95}{dish}+\frac{0}{plate}+\frac{0}{container}\right\}$ |
| SADR010624 | 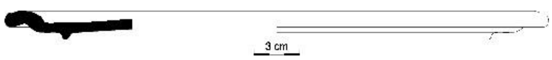  | Plate | $\left\{\frac{0}{cup}+\frac{0}{bowl}+\frac{0.04}{dish}+\frac{0.92}{plate}+\frac{0}{container}\right\}$ |

| | | | |
|---|---|---|---|
| SADR011208 | 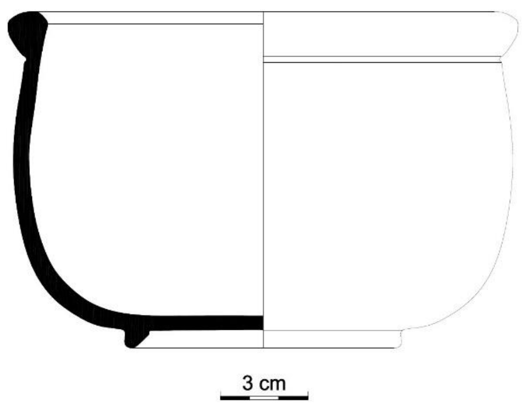 | Container | $\left\{\frac{0.05}{cup}+\frac{0}{bowl}+\frac{0}{dish}+\frac{0}{plate}+\frac{0.70}{container}\right\}$ |

To compare the fuzzy FG set with the expert's label and investigate how the original labels coincide with the algorithmic, we retain for each of the 288 profiles the class with the maximum support value. The results are provided in ***Table 2.*** The confusion matrix shows the labels that coincide in the diagonal and the pairwise mismatches are placed in the upper and lower triangle. In the current model, cups are mostly 'misinterpreted' over all classes, achieving 78% class sensitivity and the mismatches are containers (3/5) and bowls (2/5). Dishes achieve a higher class sensitivity (91%), and when they are misinterpreted this is almost exclusively for bowls (12/13) while misinterpreted bowls are rather cups (4/7). It is notable that plates have not been misinterpreted for any other crisp class and no label of the material specialist has changed by the model in the plate label. Looking at the false discovery rate, the proportion of the misinterpreted containers with respect to the available data is the largest (36%), followed by cups and bowls while for dishes the proportion can be considered negligible. Overall, the transformation of the FG label obtains 91.32% accuracy by taking into account six algorithmically retrieved geometric measures referring to the global vessel shape. However, the empirical distributions of the six geometric measures are complicated hence the model is far from straightforward, as it was also observed in the articulation of the if-then rules. Further modifying the fuzzy modelling approach could improve the results while also reflecting better the conceptual typological model and considering the sufficiency of the currently selected six geometric measures in FG analysis.

***Table 2*** *Expert's label versus crisp algorithmic class. The number of complete profiles included in the analysis, the sensitivity and the specificity of the FIS are reported per class*

| Expert's Label | Maximum support FG | | | | | Class Sensitivity | False Discovery Rate | Profiles |
|---|---|---|---|---|---|---|---|---|
| | Cup | Bowl | Dish | Plate | Container | | | |
| Cup | 18 | 2 | 0 | 0 | 3 | 78% | 22% | 23 |
| Bowl | 4 | 89 | 2 | 0 | 1 | 93% | 14% | 96 |
| Dish | 1 | 12 | 126 | 0 | 0 | 91% | 2% | 139 |
| Plate | 0 | 0 | 0 | 23 | 0 | 100% | 0% | 23 |
| Container | 0 | 0 | 0 | 0 | 7 | 100% | 36% | 7 |

Regarding the cases where the crisp algorithmic class and the expert's label do not coincide, we provide further information in ***Table 3***. These are examples that do not possess typical morphological characteristics of the functional class specified by the expert, but at the same time they do not possess the typical characteristics of any other functional class.

***Table 3*** *Mismatches of the crisp algorithmic class and expert's label*

| **ID** | **Profile** | **Expert's Label** | **FIS crisp result** | **Fuzzy FG set** |
|---|---|---|---|---|

| | | | | |
|---|---|---|---|---|
| SADR010965 | 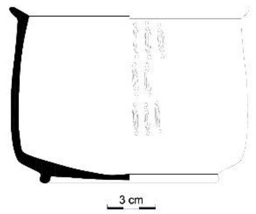 | Cup | Container | $\left\{\frac{0.18}{cup}+\frac{0}{bowl}+\frac{0}{dish}+\frac{0}{plate}+\frac{0.38}{container}\right\}$ |
| SADR010961 | 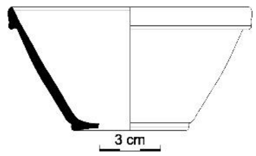 | Bowl | Container | $\left\{\frac{0.15}{cup}+\frac{0.04}{bowl}+\frac{0}{dish}+\frac{0}{plate}+\frac{0.31}{container}\right\}$ |
| SADR010684 | 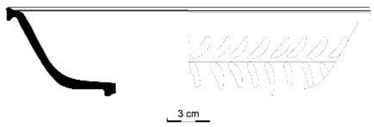 | Dish | Bowl | $\left\{\frac{0}{cup}+\frac{0.11}{bowl}+\frac{0.04}{dish}+\frac{0}{plate}+\frac{0}{container}\right\}$ |
| SADR021111 | 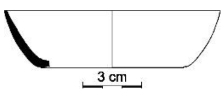 | Dish | Bowl | $\left\{\frac{0.09}{cup}+\frac{0.52}{bowl}+\frac{0.24}{dish}+\frac{0}{plate}+\frac{0}{container}\right\}$ |
| SADR021859 | 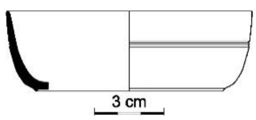 | Dish | Cup | $\left\{\frac{0.19}{cup}+\frac{0.05}{bowl}+\frac{0.07}{dish}+\frac{0}{plate}+\frac{0}{container}\right\}$ |

The transparency of the process allows to track why each support value was attributed are provides details on which morphological characteristics are non-typical. An example, specifically profile SADR010965, is worked out in ***Fig. 6***. The support of each membership function indicates that the profile resembles more a container because of its size and wall thickness, while in the size-independent properties it resembles more a cup than a container. The specific profile is labelled as 1A150, a typically large cup type (commonly 11 cm – 16 cm rim diameter) in SRSW. The rim diameter of this vessel is 14.11 cm, therefore quite typical while the wall thickness (4.86 mm) is close to the upper typical margin (5 mm) for this type. The profile cannot therefore be considered abnormal for its type, but its size is in all cases more typical for container than cup, as it can also be seen in ***Fig. 6***. The fact that the size of this cup is relatively atypical was recognized already during the creation of the original model, however the lip of this form is interpreted as easy to drink from and that had more weight in the decision making of the material specialist who originally attributed to this form the label of a cup. It follows that when this form is smaller in size, it fit more to the wider logic of 'cups', as in containers for an individual beverage.

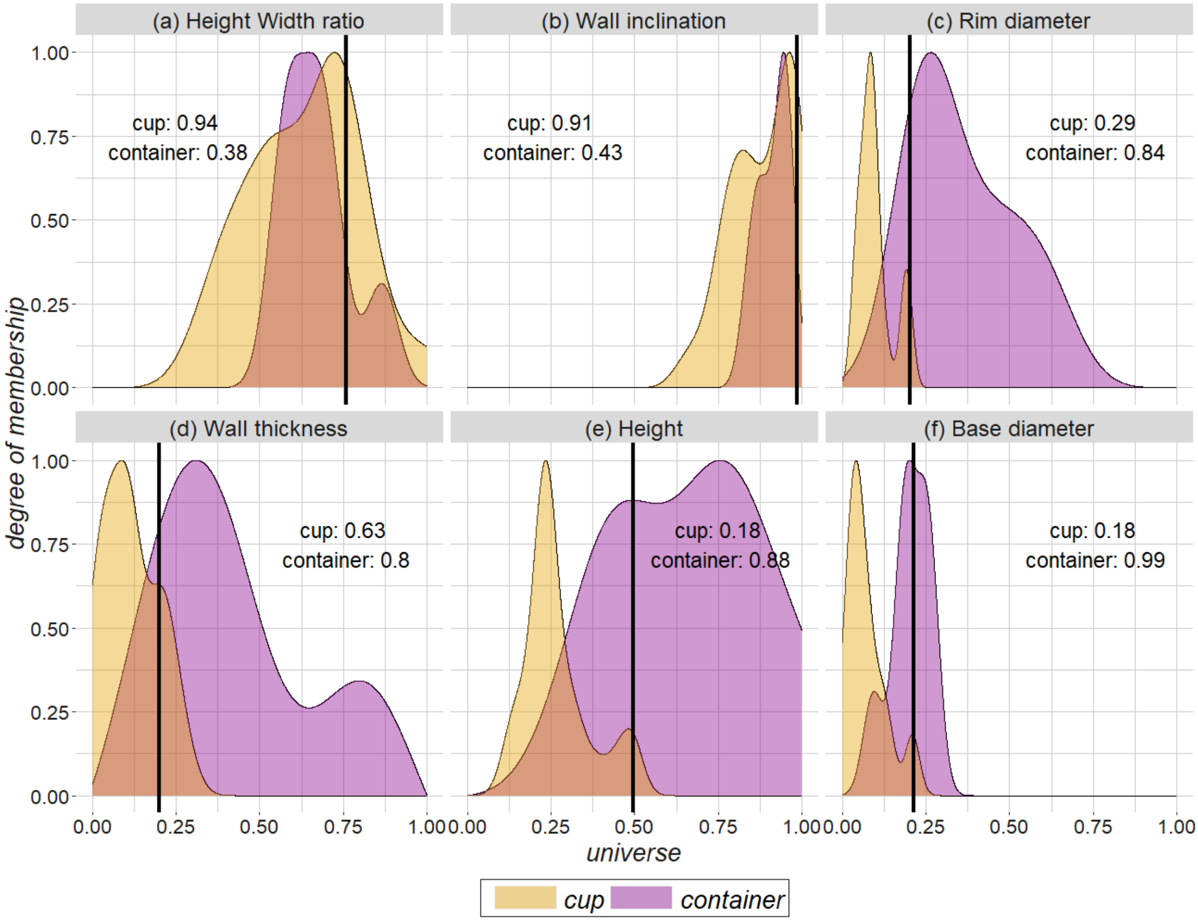


***Fig. 6*** *Results on the membership functions for profile SADR010965, labelled as 'cup' by the expert while the digital model indicates the profile is morphologically more similar to a 'container'*

In a similar manner, we may inspect the results for, what we call in our setting, a marginal case, profile SADR021860 for which the output fuzzy set is $\left\{\frac{0.06}{cup}+\frac{0.28}{bowl}+\frac{0.29}{dish}+\frac{0}{plate}+\frac{0}{container}\right\}$ and is labelled as dish by both the expert and the digital model. In the dimension-dependent variables as well as in wall inclination, this profile is in all five cases morphologically closer to a dish than a bowl, while the height/width ratio value points more towards a bowl. It is interesting that the material specialist also characterizes this profile as an atypical example of type 1C100 where the tilt of the wall could be somewhat peculiar. In the results section 'The case of SRSW 1C100', we study further potential morphological sub-groups within SRSW 1C100.

Already during the development of the original typological model there were types, such as 1B230, for which it was clear from the outset this group contained members which were better considered as dishes. But, as originally explained, there were no cut-off points to discriminate two clear groups as bowls or dishes within this type. Hence the decision to label these under the majority of appearances, as bowls in this case, fully knowing that a set of sherds were clearly dishes. Our proposal evaluates each profile with respect to its morphological resemblance to the wider SRSW class FG and sheds light to such cases.

## Fuzzy type-variants within a type

In this section, we analyze some of the popular SRSW types with no variants in the original typological model but which, according to the material specialist and their experience with the growing datasets, exhibit internal morphological variation. The aim is to propose subgroups and split each type into variants, as long as the proposed sub-groups capture archaeologically relevant information. Four types are analyzed, namely, SRSW 1F150, SRSW 1B150, SRSW 1A130 and SRSW 1C100, for which all profiles were acquired during excavations between years

1992 and 2021. A vessel of each type is shown in ***Fig. 7***. In total, 88 contexts[1] are incorporated in the analysis, of which 41 contexts include SRSW 1F150, 44 include SRSW 1B150, 49 include SRSW 1A130, and 16 include SRSW 1C100. The selected archaeological contexts are labeled with respect to their chronology, and they are selected based on their assessment by material specialists as high-quality assemblages representative for Roman material culture in Sagalassos.

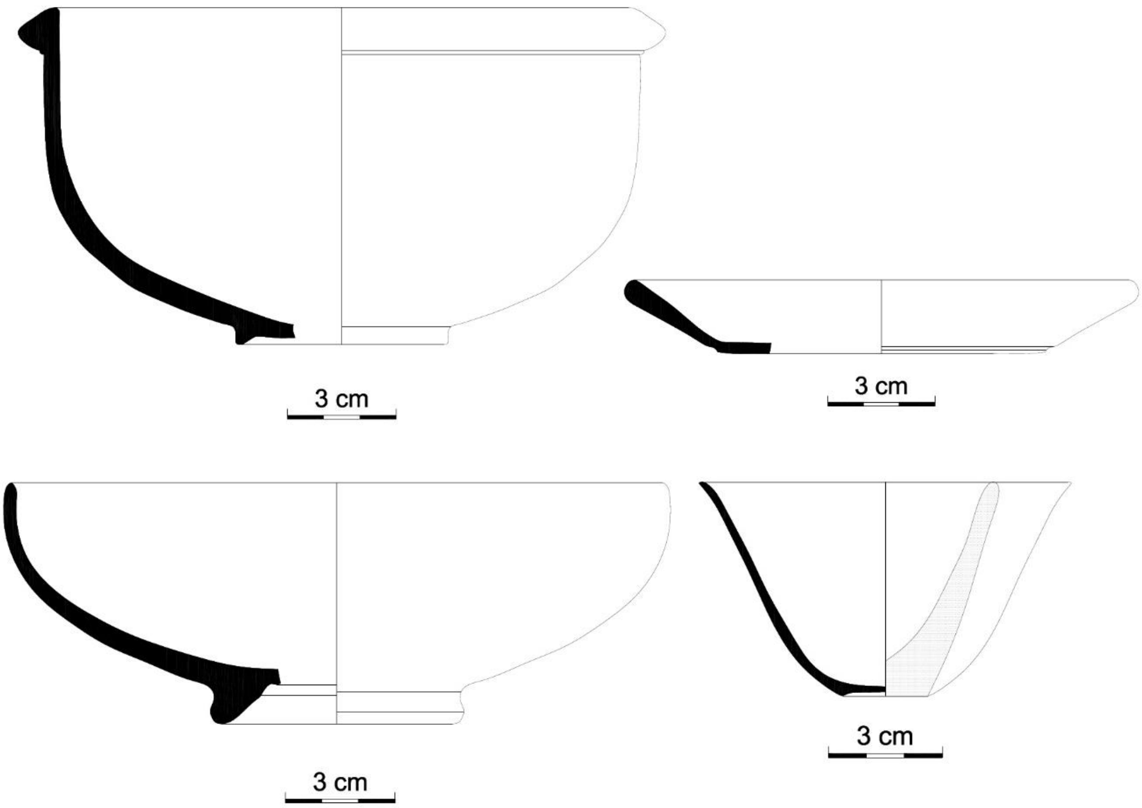


***Fig. 7*** *A complete profile for each SRSW type studied in this section: (top left) SRSW 1F150, (top right) SRSW 1C100, (bottom left) SRSW 1B150, and (bottom right) SRSW 1A130.*

In this study, we consider chronologically and non-chronologically sensitive explanations for the proposed subgroups. Some of the observed intra-type morphological modes might arise from the nature of the production process. Different smaller scale workshops were active at the same time. Each of these produced a given number of SRSW types, but likely never the full range of types available in any given period. Still, this resulted in different workshops and different potters making the same types, or at least their versions of those types, inevitably resulting in morphological variation. Given the current state of the archaeological evidence, however, this level of resolution remains difficult to grasp. Chronological variation may be induced due to changing preferences in taste or fashion and ways of doing over time, or the coming and going of workshops through time, but even within a single workshop, differences in morphology could correspond to such intractable matters as the evolving dexterity of potters.

Following our methodology, the profiles with similar morphological characteristics end up close in the quantified space and cluster together, therefore we examine whether the resulting clusters inherit a temporal interpretation. Especially in such cases, we should consider the information relevant to capture in the SRSW typology, following the algorithmically proposed variants of the type.

To assess the chronological relevance of the results, we make use of the assemblage-based chronological label, as provided by the material specialist during field work. The chronological label refers to SRSW Phases 1 – 9 (Poblome, 1999; Poblome et al., 2010) (see ***Table 4***) and is given to each of the 88 contexts included in this

[1] The context ID used from here onwards, follows the format SA-YYYY-XXXX-00000 in accordance with the labelling practices of archaeological contexts in the Sagalassos Archaeological Research Project.

section. When the label of the context is broader than a specific Phase, the profiles found in this context are split accordingly. For instance, if one profile is found in a context labelled as SRSW Phase 1–2, then, the profile is uniformly split in Phase 1 and Phase 2. The types we work with in this section are mostly from the Early Roman Imperial to Roman Imperial (Phase 1 – 5) period, while some occur in contexts of the Late Roman period.

***Table 4*** *Phases of SRSW, associated dates and times*

| SRSW Phase | Lower date | Upper date | Times |
|---|---|---|---|
| Phase 1 | 25 BCE | 50 CE | Early Roman Imperial |
| Phase 2 | 50 CE | 100 CE | |
| Phase 3 | 100 CE | 150 CE | Roman Imperial |
| Phase 4 | 150 CE | 200 CE | |
| Phase 5 | 200 CE | 300 CE | |
| Phase 6 | 300 CE | 350/375 CE | Late Roman |
| Phase 7 | 350/375 CE | 450/475 CE | |
| Phase 8 | 450/475 CE | 550/575 CE | Early Byzantine |
| Phase 9 | 550/575 CE | 700 CE | |

For each type we study, the sources of morphological variation, the breakage patterns, etc., are different, resulting in different choices for the morphological quantification. Considering that the nature of fabric and slip are fairly consistent for all SRSW types, the form plays an important role in how vessels break into pieces. Based on our digitally available sample, the base is usually missing from the SRSW 1F150 and SRSW 1A130 finds. It is important to mention that there are only a few basic base types, making unique links between bases and the rest of the sherds very difficult. SRSW 1B150 breaks relatively more since in several cases only the upper half of the wall is found while SRSW 1C100 profiles are found more often complete than incomplete. Based on the material specialist's observations and developed theory for the within-type morphological variation, we will explore different morphological properties in each of the considered case studies. For SRSW 1F150, we will explore size variation. For SRSW 1B150, the presumed sources of morphological variation are the rim form, upper wall form and overall size. Finally, in SRSW 1A130 and SRSW 1C100, we are interested in the variation of the overall form of the profile, independent of the size.

Taking the above into account, our choices regarding morphological quantification of the profiles evolves as follows. For SRSW 1F150, we use the rim diameter as a proxy to measure the size of the profile. For SRSW 1B150, the 1D outline transformation is used to quantify the rim form. We also use the global geometric measure of wall inclination below the rim as a proxy to quantify the form of the upper wall and the rim diameter to quantify the size. For SRSW 1A130, we study sherds of equal length containing the rim and part of the wall (the rim of SRSW 1A130 is rather indistinguishable from the upper wall) and for SRSW 1C100, we proceed with the complete profiles.

In each case study presented in this section, we provide the description of the type from the original typology, the clustering results including algorithmically proposed variants with central/peripheral/marginal cases, the morphological description of each cluster, and archeological interpretation.

**The case of SRSW 1F150**

The SRSW 1F150 is a type of open container with distinctive horizontally folded rim form and is rarely found complete (Poblome, 1999, p. 170). This type is produced from Phase 1, soon becomes popular and is considered residual from Phase 7 onwards. To measure the size of the profile when mostly incomplete examples are available, we use the rim diameter as a proxy. In total, 73 profiles with known rim diameter, are analyzed.

In this one-parameter (rim diameter) implementation, the absolute difference (Manhattan distance) - which coincides with the Chebyshev, Euclidean and Minkowski distance values - between the rim diameter of each pair of profiles is best at capturing (dis)similarity. The fuzzy clustering methodology is implemented for $k = 2$ and the resulting crisp clusters include 54 and 19 members, respectively delineating a more popular smaller version of this type versus a larger variant. As visualized in ***Fig. 8***, the first sub-group contains profiles with lower rim diameter, minimum 9.30 cm and maximum 20.70 cm with a median of 14.95 cm and a mean of 14.40 cm. The second sub-group contains profiles with a median rim diameter of 27.11 cm, mean 26.81 cm, minimum 22.77 cm and maximum 30.71 cm.

The location of the central and peripheral members of each fuzzy cluster are in line with the summary statistics observed for the rim diameter values of each crisp cluster. Namely, fuzzy cluster 1 includes 5 members with support higher than 0.99 and rim diameters of 13.78 cm, 14.09 cm, 14.13 cm, 14.49 cm and 14.53 cm. Central members for fuzzy cluster 2 and support higher than 0.99 have 26.37 cm, 27.11 cm and 27.30 cm rim diameter. The peripheral members are close to the gap observed in the rim diameter values and these possess the maximum and minimum rim diameter values of crisp clusters 1 and 2 respectively. However, the support for the profile of diameter 20.70 cm belonging to crisp cluster 1 is 0.55, considerably lower than the peripheral member of crisp cluster 2 which has support 0.77. No marginal cases occur in the fuzzy clustering results for SRSW 1F150.

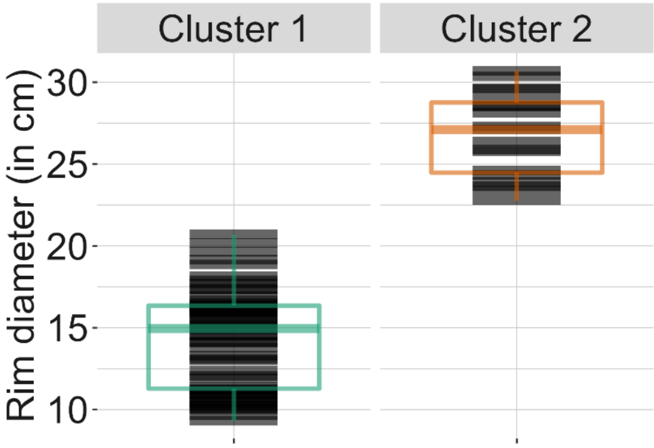


***Fig. 8*** *Rim diameter (in cm) and boxplot for all SRSW 1F150 profiles per crisp cluster.*

The variants of this type signify chronological importance with a shift from the larger to the smaller variant peaking during Phase 3. ***Table 5*** shows that the majority (61%) of the smaller containers are found in contexts of Phase 3 or later while 79% of the larger containers are found in contexts of Phase 1 and 2. It is also interesting that 61% of the containers found in contexts of Phase 3 have rim diameter less than 11.90 cm and the rest have more than 14.88 cm rim diameter. In that sense, Phase 3 1F150 profiles are not the most representative of the proposed cluster-1; the smaller containers of Phase 3 belong with support 0.89 – 0.97 in cluster-1 and the largest profiles with support 0.88 – 0.98 while three out of five most representative profiles of cluster-1 come from Phase 2.

If we zoom in on some of the Phase 3 1F150 profiles, we see that 16 are derived from the same context (SA-1997-PQ-00006), which is part of a dump of non-approved pottery that was never sold or used. These pots were not misfired, but were seen as displaying some sort of default that made them unsuitable for selling. We have to be aware therefore that the observed pattern may be in part determined by the output of one of the workshops and is not necessarily directly related to aspects of pottery production or consumption. Still, it is important to point out that by studying a local production center, and thus incorporating not only consumption but also patterns of production, we can provide an enriched picture compared to many other studies. The fact that the observed cluster is not limited to Phase 3, and that the most typical cases are actually found in Phase 2, suggests that the pattern captures a historical reality of the production process and some underlying chronological salience.

***Table 5*** *Proportion of 1F150 profiles per cluster for each SRSW Phase.*

| SRSW Phase | Cluster of SRSW 1F150 | | Profile Count (Phase) |
|---|---|---|---|
| | 1 | 2 | |
| Phase 1 | 20.4% | 44.7% | 19.5 |
| Phase 2 | 19.0% | 34.2% | 16.8 |
| Phase 3 | 34.4% | 8.8% | 20.3 |
| Phase 4 | 2.9% | 3.5% | 2.3 |
| Phase 5 | 15.9% | 8.8% | 10.3 |
| Phase 6 | 2.8% | 0.0% | 1.5 |

| | | | |
|---|---|---|---|
| Phase 7 + | 4.6% | 0.0% | 2.5 |
| Profile Count (Cluster) | 54 | 19 | Grand Total 73 |

**The case of SRSW 1C100**

In the original typological model (Poblome, 1999, p. 106), type 1C100 is described as a ‘small dish with outspread, straight or slightly concave walls, ending in a disc base which can be slightly concave. A carination in the bottom part of the walls, towards a ring base, or, mostly a disc base, is common. The rim is plain, rounded or slightly thickened’. This is a common type and is considered traditional in the eastern Mediterranean, with parallels in Eastern Sigillata A and Eastern Sigillata C. From the original typological model, it is given that the type was most popular in Phase 5 and it occurred from Phase 1 to Phase 6.

Several full profiles were already available during the making of the original typological model, and in the current collection of digital drawings, full profiles are more abundant than rim profiles. We are therefore analyzing complete profiles, using the 1D profile transformation for $L = 300$. The distance selection process indicates that the Manhattan metric is best capturing local and global relationships of vessels and the network map in ***Fig. 9*** (seed = 616) is created with 77 edges on the 47 nodes, and Shepard $R^2 = 0.79$. The nodes are colored according to the clustering results, where the vessels are grouped in three clusters of sizes 11, 27, and 9.

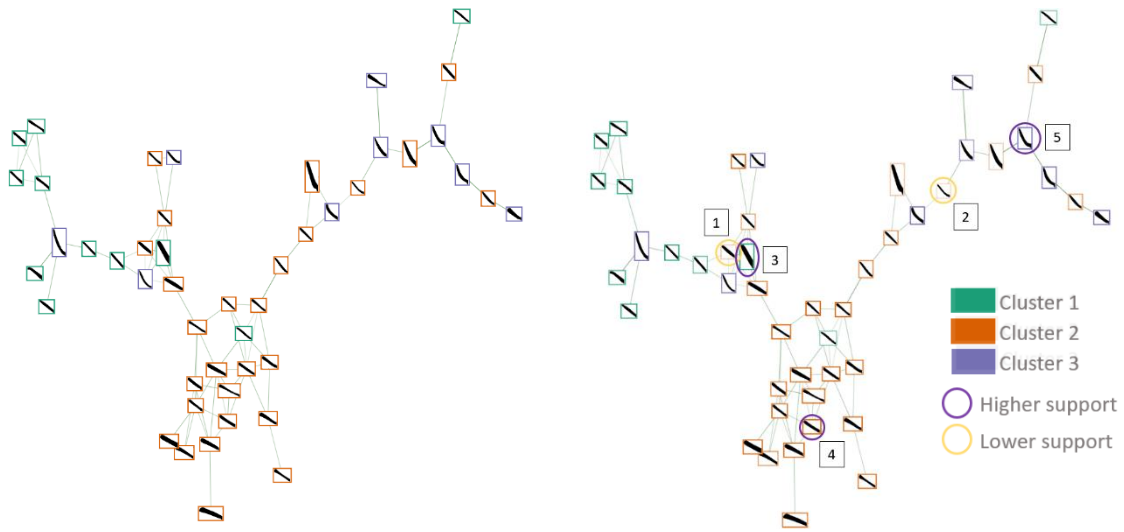


***Fig. 9*** *Network map of 1C100 with the corresponding rim images as nodes, colored and annotated according to the fuzzy clustering result: (left) color hue with regard to the crisp cluster class and uniform opacity, (right) opacity of the node stroke with regard to the support value.*

Although in the network map vessels of cluster-3 seem more scattered, in fact cluster-2 is more loosely defined compared to the rest, having 0.44 minimum and 0.97 maximum support for vessels belonging to crisp cluster-2. Cluster-1 has a larger minimum support for the vessels it encompasses, namely 0.64 and maximum 0.97 while vessels belonging to crisp cluster-3 have support values between 0.72 and 0.98. There are no marginal cases. However, more attention should be given to the profiles with ID 1 (Phase 2) and with ID 2 (Phase 5), as there are only small differences in the support values. ID 1 has support 0.51 in cluster-2 and 0.45 in cluster-1 and ID 2 is included with the minimum support in cluster-2 and belongs to cluster-3 with support 0.41.

The 1D profile is plotted per cluster in ***Fig. 10***. Visually, we detect two profiles in cluster-3 that deviate from the overall pattern in the wall angle at the upper part of the profile. However visually, they still fit in cluster-3 because they do have a concave wall. Interestingly, these two are not showing low support in belonging to crisp clsuster-3.

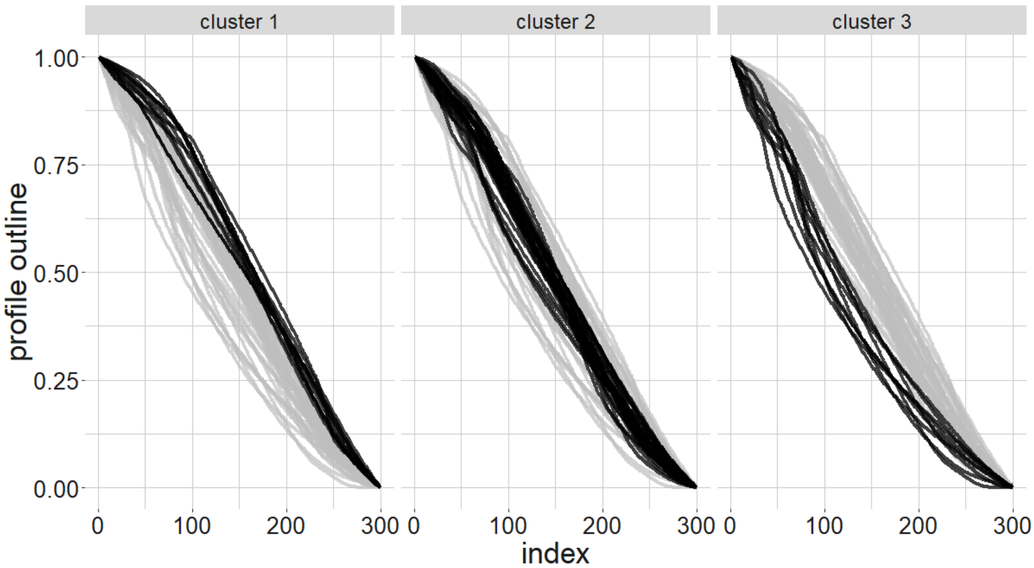


*Fig. 10* *One-dimensional GAM per crisp cluster in SRSW 1C100*

From the set of global geometric measures, only the position of the wall angle differs significantly between all groups. On average, the wall bends most in cluster-1 at 85% of the height, in cluster-2 at 69% of the height and at cluster-3 at 46% of the height. The inclination is significantly different between cluster-2 and cluster-3, and is larger by 0.1 on average in cluster-3. The ratio between the position of the maximum diameter and the height differs significantly between cluster-1 and cluster-2, which means that the maximum diameter is generally found higher in vessels belonging mostly to cluster-1 than the vessels belonging mostly to cluster-2.

The algorithmically proposed variants hold relevant chronological information (see **Table 6** Proportion of 1C100 profiles per cluster for each SRSW Phase***Table 6***). Cluster-1 seems to capture a trend in Phase 2, judging by 91% of profiles derived from four contexts out of the five in this cluster. The vessels with the highest membership are from contexts both from Phase 1 and Phase 2 for cluster-1, from contexts labelled as Phase 3 and one Phase 5 for cluster-2, and from contexts of Phase 2 and Phase 3 for cluster-3. This observations shows a plausible trend of variant-1 being earlier than variant-3 and variant-2 being later compared to the other 2 variants.

Another interesting observation is that the amount of vessels in Phase 5 or later is not high, compared to the frequency of vessels for the other SRSW Phases. However, to judge whether the type is still most popular in Phase 5, another type of analysis is needed which would take into account the relative popularity of the type within Phase 5 contexts.

***Table 6*** *Proportion of 1C100 profiles per cluster for each SRSW Phase*

| SRSW Phase | Cluster of Type 1C100 | | | Profile Count (Phase) |
|---|---|---|---|---|
| | 1 | 2 | 3 | |
| Phase 1 | 9% | 10% | 31% | 6.5 |
| Phase 2 | 91% | 27% | 36% | 20.5 |
| Phase 3 | 0% | 38% | 26% | 12.5 |
| Phase 4 | 0% | 1% | 4% | 0.5 |
| Phase 5 + | 0% | 25% | 4% | 7 |
| Cluster Count (Cluster) | 11 | 27 | 9 | 47 |

**The case of SRSW 1B150**

In its initial textual description (Poblome, 1999, p. 61), SRSW 1B150 is a ‘very small or larger bowl with convex walls curving towards a ring-base and plain, rounded or slightly thickened rim. The walls can curve towards a vertical position. Open form. Occasionally the exterior rim and body are grooved. No decorated examples found'. It is also given that type 1B150 was most popular in Phase 2 of SRSW but was already produced in Phase 1 while it was still popular until Phase 5 with a tendency towards increasing sizes.

From the available sample, there are 20 complete profiles out of 104 while 94 have known rim diameter and are used in the analysis. To quantify the form of the 94 profiles, we use the 1D outline transformation for the rims and two geometric measures, namely rim diameter and inclination below the rim. First, we compute the distance matrices for the 1D outline transformation ($L = 355$) and select the Chebyshev distance metric following the distance selection process. Second, we consolidate the Chebyshev distance matrix, retaining four eigenvalues from *PCA* explaining 94.65% of the total variance, with the two selected global geometric measures, ending up with the consolidated data of 6 variables and 94 observations. We again follow the distance metric selection method for the consolidated data, which suggests that the (dis)similarity between profiles is best captured using the Manhattan metric. Next, we apply the network embedding algorithm (seed = 629) and we retain 116 edges on the 94 nodes. The network map (Shepard $R^2 = 0.84$) is shown in ***Fig. 11***.

We also implement the fuzzy clustering methodology for k = 3 on the distance matrix of the consolidated data, which suggests groups of 23, 45 and 26 sherds for crisp cluster class 1, 2 and 3 respectively. The nodes of the network map are colored accordingly in ***Fig. 11***. Next, within each cluster we identify central, peripheral, and marginal cases. The network map is annotated with respect to this information.

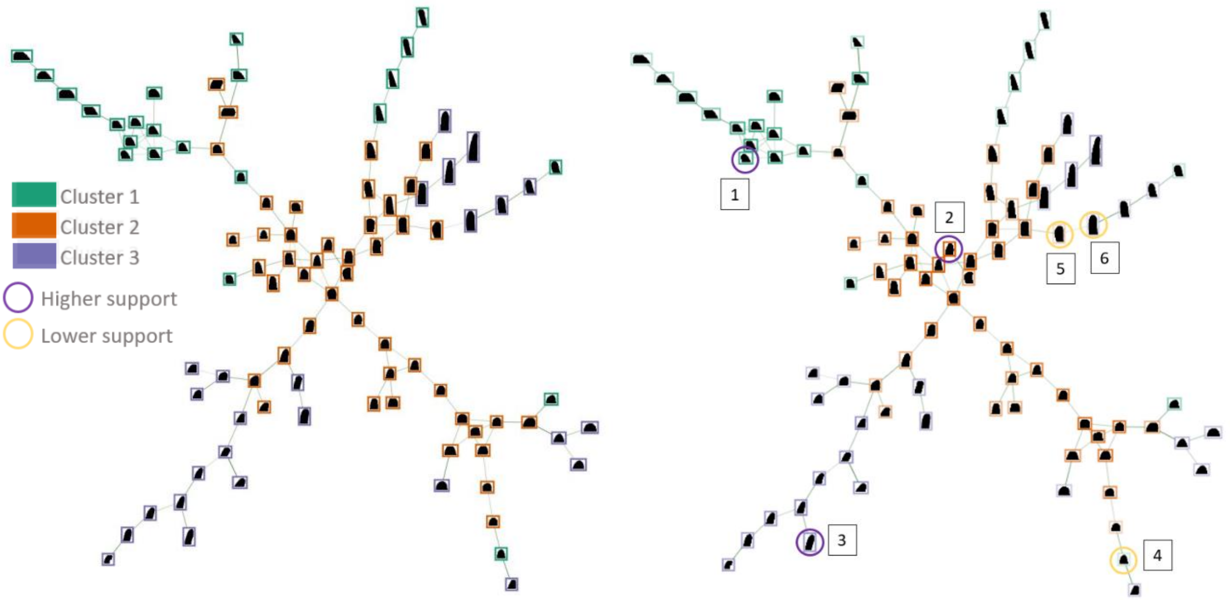


***Fig. 11*** *Network map of 1B150 with the corresponding rim images as nodes, colored and annotated according to the fuzzy clustering result: (left) color hue with regard to the crisp cluster class and uniform opacity, (right) opacity of the node stroke with regard to the support value.*

All three clusters have comparable ranges of support values for the sherds belonging mostly to each of them. Cluster-1 has support values from 0.37 to 0.75, cluster-2 has 0.40 to 0.82, and cluster-3 has 0.37 to 0.69. Sherds annotated with IDs 1, 2 and 3 are the most central for each cluster class and sherds with ID 4, 5 and 6 are the most peripheral, while there are no marginal cases. The most central case in each crisp clusters belongs to context SA-2003-LA2-00080 labelled as Phase 2 for cluster-1, SA-2006-SS1-00151 labelled as Phase 1 for cluster-2 and SA-2004-PQ-00071 labelled as Phase 1 for cluster-3. This information is taken into account for assessing the chronological relevance of the results at the end of this case study.

To shed light on the morphological characteristics of the 1B150 sherds, we first present the 1D rim outlines per crisp cluster and their median in ***Fig. 12***. We do not expect the 1D outlines to be completely grouped together in the quantified space, since the grouping is based additionally on two geometric measures. Looking at ***Fig. 12*** we observe that the outer part of the outline is generally broader within each crisp cluster than the inner part, and that the outer part also exhibits more overlap than the inner. It is notable that profiles in cluster-1 span almost the complete quantified space at the outer part while at their inner part, the 1D outline concentrates more in the upper plot area. For all three clusters, the inner part is on average distinct at the last indices, with the 1D outlines of cluster-1 sherds being further away for the rim top than the rest and the 1D outlines of cluster-3 sherds being closer to the rim top than the rest.

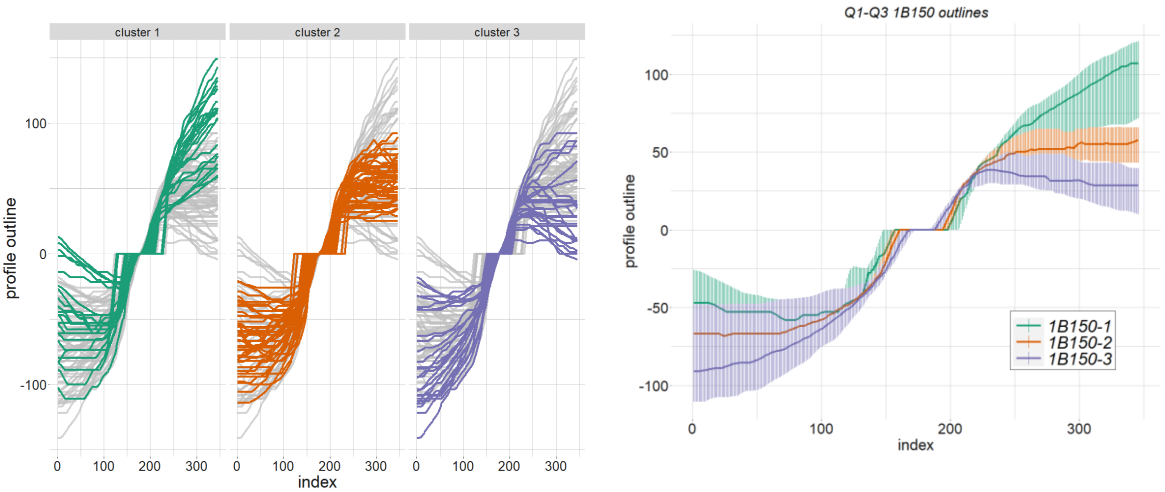


*Fig. 12* *(left) Superimposed sherd outlines coloured and faceted by cluster (right) First quartile, median and third quartile of the outlines computed per index and by cluster.*

Besides rim outlines, the grouping results are also determined by the rim diameter and the inclination below the rim. An overview of the geometric measures by crisp cluster class can be found in ***Table 7***, along with additional geometric measures. The average of the rim diameter is different in all groups, with cluster-1 having, on average, the smallest, and cluster-3 having the largest. Sherds in cluster-1 have considerably smaller rim diameters on average, with 13 sherds having rim diameters between 6.27 cm and 7.1 cm, 3 sherds having a value close to the mean, a group of 5 sherds having values between 11.1 cm and 11.9 cm and exhibiting one potential outlier with rim diameter 19.83 cm. Sherds in cluster-2 have a smaller range than sherds in cluster-1 and the spread of the middle half of the data is between 11.77 cm and 15.73 cm. Sherds in cluster-3 have the broadest range of values spanning the complete empirical area of the variable, but the spread of the middle half of the data is between 13.18 cm and 18.55 cm.

The average of the inclination below the rim is negative for all clusters. This indicates that below the rim, the general trend for all clusters is for the wall to form a smaller than 90-degrees angle with the x-axis of the Cartesian coordinate system (see ***Fig. 3***). The angle is significantly smaller in cluster-1, meaning that on average the walls of the sherds in cluster-1 are more outspread than the wall of sherds in cluster-2 and cluster-3. The range of values shows a similar pattern to that of the rim diameter, with sherds in cluster-3 spanning almost the complete area of empirical values.

***Table 7*** *Pairwise difference of group means and significance of the difference. Average value per geometric measure per cluster of 1B150.*

| Geometric measure | clusters 1 - 2 | clusters 1 - 3 | clusters 2 - 3 | Cluster-1 | Cluster-2 | Cluster-3 |
|---|---|---|---|---|---|---|
| Aspect ratio | 0.499 (**) | 0.05 | 0.549 (***) | 2.426 | 1.927 | 2.476 |
| Block % | 3.833 (*) | 0.933 | 2.9 | 84.378 | 88.212 | 85.312 |
| Curl | 0.166 | 0.306 (***) | 0.14 (*) | 2.692 | 2.526 | 2.385 |
| Eccentricity | 0.061 | 0.072 | 0.133 (***) | 0.716 | 0.655 | 0.788 |
| Elongation avg | 0.095 | 0.464 (*) | 0.369 | 1.423 | 1.518 | 1.887 |
| Elongation max | 0.14 (*) | 0.435 (*) | 0.295 | 1.157 | 1.297 | 1.592 |
| Elongation min | 0.921 | 3.063 (**) | 2.142 (*) | 3.384 | 4.305 | 6.447 |
| Extent 1 | 0.047 (**) | 0.021 | 0.026 | 0.816 | 0.864 | 0.837 |
| Form factor | 0.024 | 0.042 | 0.066 | 0.939 | 0.963 | 0.897 |
| Inner difference length | 0.084 (***) | 0.128 (***) | 0.044 (*) | 0.175 | 0.091 | 0.047 |

| | | | | | | |
|---|---|---|---|---|---|---|
| Inner difference length (max) | 0.075 (***) | 0.069 (***) | 0.005 | 0.175 | 0.101 | 0.106 |
| Inner protuberance length | 0.015 | 0.018 | 0.003 | 0.016 | 0.031 | 0.034 |
| Maximum wall thickness | 0.029 | 0.036 | 0.007 | 0.333 | 0.362 | 0.369 |
| Median wall thickness | 0.046 | 0.041 | 0.004 | 0.289 | 0.335 | 0.331 |
| Outer difference length | 0.103 (***) | 0.185 (***) | 0.082 (***) | -0.020 | -0.123 | -0.205 |
| Outer difference length (max) | 0.054 (**) | 0.133 (***) | 0.079 (***) | 0.080 | 0.134 | 0.213 |
| Outer protuberance length | 0.02 (*) | 0.02 (*) | 0 | 0.026 | 0.047 | 0.047 |
| Profile rim diameter (in cm) | 4.322 (***) | 6.724 (***) | 2.401 (*) | 9.051 | 13.374 | 15.775 |
| Radius ratio | 0.293 | 1.015 (*) | 0.723 (*) | 2.930 | 3.223 | 3.945 |
| Rim height (in cm) | 0.09 (*) | 0.214 (**) | 0.123 | 0.368 | 0.459 | 0.582 |
| Rim top flatness | 0.008 | 0.026 | 0.034 (*) | 0.177 | 0.184 | 0.150 |
| Roundness | 0.106 (***) | 0.019 | 0.125 (***) | 0.500 | 0.606 | 0.481 |
| Inclination below rim | 0.032 (***) | 0.054 (***) | 0.022 | -0.063 | -0.031 | -0.009 |
| Trapezoid % | 6.598 (*) | 10.995 (***) | 4.397 | 110.888 | 117.486 | 121.883 |

It is interesting that the geometric measures for ‘inner difference length’ and ‘outer difference length’ exhibit statistically significant differences between all clusters. It follows that for both the inner and the outer part of the 1D outline, there is an algorithmically distinguishable difference between the distance of the rim top and the rim base. Also, the rim height is smaller for sherds in cluster-1.

To morphologically describe each cluster, we also present the fuzzy description results on SRSW functional label and rim, per crisp cluster. We can only attribute fuzzy functional description to the complete profiles. For 1B150, all complete profiles are described as bowls from the algorithmic model, except for two, for which we provide a summary in Appendix, from section ‘Fuzzy functional interpretation based on global shape’.

The main results on rims are as following. As shown in ***Fig. 13***, the rims are mostly (76%) straight, with cluster-2 being dominated by straight rims (91%), followed by cluster-1 (70%). In cluster-3, ambivalence prevails since rims are straight by 54%, inverted by 42% and everted by 4%. However, the everted rim in cluster-3 has low support (0.035) and all other everted rims belong to cluster-1.

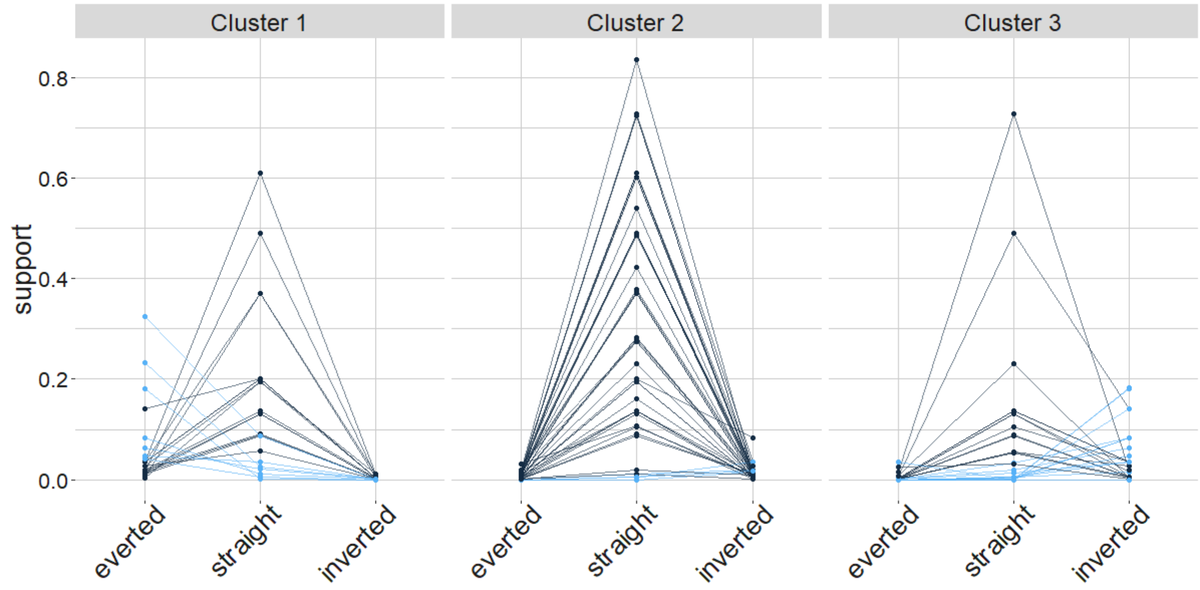


***Fig. 13*** *Parallel coordinates plot showing the support values for $\widetilde{Set_1}$ per profile and its crisp cluster. The line is colored light blue for the profiles that have higher support for inverted or everted.*

As shown in ***Fig. 14***, rims are mostly plain (91%), only one is thickened in cluster-1 while thinned rims are scattered across all three clusters. As in the previous polythetic descriptor with straight rims, we also observe here that plain rims have higher support than other descriptors.

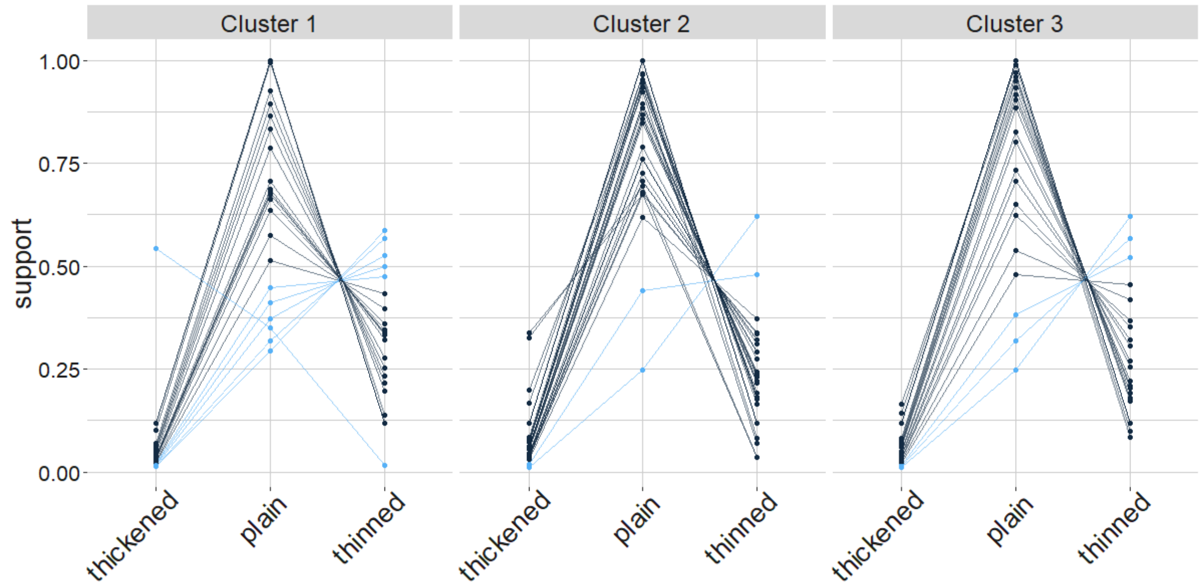


***Fig. 14*** *Parallel coordinates plot showing the support values for $\widetilde{Set_5}$ per profile and its crisp cluster. The line is colored light blue for the profiles that have higher support for thickened or thinned.*

The morphological variants of this type again imply chronological relevance. ***Table 8*** shows that the majority (68%) of cluster-3 sherds are found in contexts of Phase 1, hence cluster-3 captures a form which is produced earlier than the other variants but, based on our morphological analysis results, this form seems to be less standardized compared to the rest. We could further argue that cluster-1 and cluster-2 capture two modes within 1B150 that are produced possibly contemporaneously, or that the form captured by cluster-2 is produced earlier than the form captured by cluster-1. Based on the original type description, type 1B150 was expected to be larger in the chronologically later variety, however this turned out not to be supported by the algorithmic analysis. We should bear in mind though that the dataset analyzed in this paper is larger than the one used for developing the original model, so it is likely that new trends would emerge. Second, it is our proposed methodological approach that teases out multivariate and subtle morphological differences that potentially have chronological salience. For the time being, there are no straightforward functional or other archaeological reasons to explain this pattern but we can further investigate these conclusions by revisiting the detail of the concerned assemblages, in order to gauge whether we need to rethink the proposed chronological ranges. Clearly, this is an exercise beyond the scope of this paper. Another point to consider for the morphological analysis of this type is the overlap that exists with other types such as (SRSW 1B170 and 1C120). A typological (re)arrangement at the level of these three types could point towards a more practical rearrangement that reduces the overlap and reinforces the identity of each type.

***Table 8*** *Proportion of 1B150 profiles per cluster for each SRSW Phase*

| SRSW Phase | Cluster of Type 1B150 | | | Profile Count (Phase) |
|---|---|---|---|---|
| | 1 | 2 | 3 | |
| Phase 1 | 24% | 41% | 68% | 43.0 |
| Phase 2 | 41% | 21% | 16% | 22.0 |
| Phase 3 | 23% | 25% | 8% | 18.7 |
| Phase 4 | 1% | 3% | 0% | 1.7 |
| Phase 5 | 10% | 5% | 8% | 6.7 |
| Phase 6 + | 0% | 4% | 0% | 2.0 |
| Profile Count (Cluster) | 23 | 45 | 26 | 94 |

**The case of SRSW 1A130**

In the original typological model (Poblome, 1999, p. 37), the morphology of SRSW 1A130 is described as: 'Deep cup with plain or slightly thinned rim and distinctive outspread walls, straight or concave'. This type has typically thin walls between 2 mm and 4 mm and it is popular during Phase 1 and Phase 2, it is still present in Phase 5 contexts while it is considered residual in Phase 6. The form of SRSW 1A130 is a traditional one in the eastern Mediterranean, continuing the Hellenistic form produced in Sagalassos (11A130) (Daems et al., 2019; Daems & Poblome, 2022; van der Enden et al., 2018), while there are parallels with Eastern Sigillata A, Eastern Sigillata B, and Eastern Sigillata C.

Since complete vessels are not common for this type (5 out of 114 are complete in our dataset), we quantify the rim and the upper wall profile, excluding the rim diameter and therefore the orientation of the rim because in this type, inferring the rim diameter from the sherd is not straightforward. We rotated the profiles such that the point C forms a 90-degrees angle with point A (see ***Fig. 3***) and we retrieve profiles of equal height, namely 1.09 cm, equal to the shortest profile so that additional profiles are not excluded from the data. The scaling is not performed in this case, since the profiles are already compared in segments of equal length. Based on the cropped and rotated profiles, we produce the 1D outline for each profile using $L = 300$, without considering the flat top in the outline since in this case, the measures value is on average 0.9 mm.

The selected distance metric is the Euclidean and the fuzzy type-definition process results to 4 clusters of sizes 40, 23, 5, and 46. Working with sherds of equal height produces a more straightforward visual summary of the profiles per cluster, by superimposing the profiles based on their point C and in the processed 1A130 also point A (see ***Fig. 3***). For the superimposed profiles in ***Fig. 15***, the summary profile area becomes darker when more individual profiles are defined in this area. As a general trend, we observe that the wall thickness is varying between clusters and that some profiles are less upright.

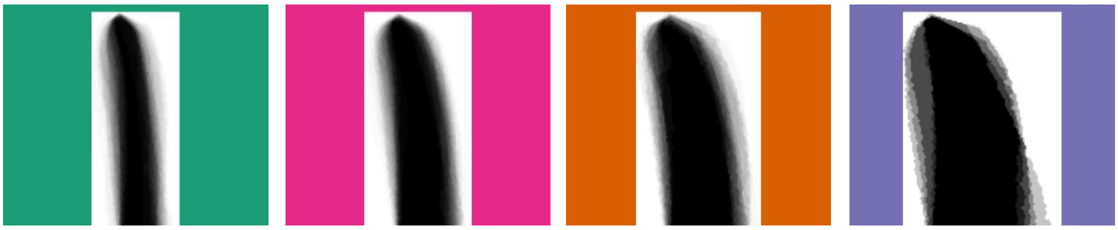

*Fig. 15* *Two-dimensional envelopes of the SRSW 1A130 morphological sub-groups*

The envelopes in ***Fig. 15*** also allow checking for profiles that deviate from the mass and seem atypical from a qualitative analysis perspective, while the complete overview of algorithmically typical and atypical profiles is based on the network map in ***Fig. 16***. The map (seed = 645) is created with 292 edges on the 114 nodes with Shepard $R^2 = 0.96$.

Profiles in cluster-3 do not seem typical 1A130 but they also do not resemble other SRSW more than they resemble 1A130. We can visually discern that profile with ID 9 in cluster-3 is considered rather atypical but is not the most peripheral in its cluster, having support 0.69 and 0.19 support in cluster-2, while the lowest support of members in cluster-3 is 0.46 with 0.35 support in cluster-2. Profile ID 9 has the second to lowest value, with the other three members of the group having 0.88 support or higher. All three clusters have comparable range of support values for the sherds belonging mostly to each of them. Cluster-1 has support values from 0.51 to 0.96, cluster-2 has 0.47 to 0.96, cluster-3 has 0.46 to 0.99, and cluster-4 has 0.46 to 0.95. Sherds annotated with IDs 1, 2, 3, and 4 are the most central for each cluster class and sherds with ID 5, 6, 7, and 8 are the most peripheral, while there are no marginal cases.

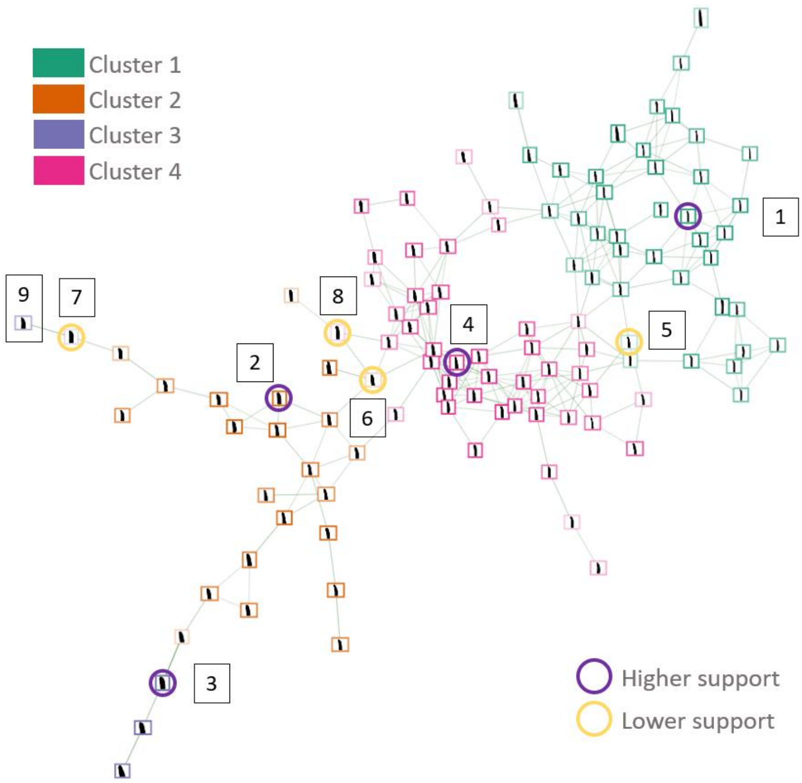


*Fig. 16* *Network map of SRSW 1A130 colored according to the crisp cluster label and the opacity is according to the support value in the crisp cluster label. The network is annotated for central and peripheral cases.*

Following the fuzzy clustering results, we present the results on fuzzy textual descriptors. The majority of straight rims (94%) belong to crisp cluster-1 and two straight rims in cluster-4 with support values 0.51 and 0.73 against 0.40 and 0.19 for belonging in cluster-1. No sherds are inverted and 69% of the total are everted but with relatively low support values. No sherd is horizontally flattened or rounded. Two are vertically flattened at the exterior and the rest not, with high support (0.99) in cluster-1, lower support (0.73) in cluster-4, only one close in the decision making in cluster-2 (support values are 0.46 and 0.54). At the interior, seven sherds are vertically flattened, specifically four, one and two in clusters-1, -2, and -4 respectively. Sherds are typically plain, one is thickened in cluster-1 and two are thinned with relatively low support, 0.52 and 0.48, in cluster-4 and cluster-2 respectively. One mismatch we observe in cluster-3 which has higher support for plain (0.49) and the second dominant class is thinned (0.45), however we would expect the result to be the other way round – thinned but also not far from plain.

Based on the statistical difference of geometric measures between clusters (see ***Table 9***), two measures differ across all groups, namely roundness and form factor. This means that a clear difference amongst groups is accounted for the relationship with the rim area and the radius or the perimeter length of the profile. We also observe that clusters-2 and -3 do not differ much on average, since 10 geometric measures (capturing wall thickness, inner difference length, and elongation) differ significantly for the rest of the pairwise comparisons but not between cluster-2 and -3.

*__Table 9__ Pairwise difference of group means and significance of the difference. Average value per geometric measure per cluster of 1A130.*

| Geometric measure | clusters 1 - 2 | clusters 1 - 3 | clusters 1 - 4 | clusters 2 - 3 | clusters 2 - 4 | clusters 3 - 4 | Cluster-1 | Cluster-2 | Cluster-3 | Cluster-4 |
|---|---|---|---|---|---|---|---|---|---|---|
| Aspect ratio | 2.667 (***) | 3.444 (***) | 1.699 (***) | 0.777 | 0.968 (***) | 1.745 (**) | 6.635 | 3.968 | 3.191 | 4.936 |
| Block % | 0.733 | 0.811 | 0.15 | 0.078 | 0.883 | 0.961 | 87.133 | 86.400 | 86.322 | 87.283 |
| Curl | 0.028 | 0.037 | 0.014 | 0.009 | 0.014 | 0.024 | 2.082 | 2.053 | 2.044 | 2.068 |
| Eccentricity | 0.038 (***) | 0.076 (***) | 0.016 (***) | 0.039 | 0.021 (***) | 0.06 (**) | 0.979 | 0.942 | 0.903 | 0.963 |
| Elongation avg | 2.273 (***) | 3.018 (***) | 1.43 (***) | 0.745 | 0.843 (***) | 1.588 (**) | 5.657 | 3.384 | 2.639 | 4.227 |
| Elongation max | 2.012 (***) | 2.652 (***) | 1.247 (***) | 0.641 | 0.765 (***) | 1.405 (**) | 4.923 | 2.911 | 2.271 | 3.676 |
| Elongation min | 7.452 | 0.101 | 7.813 | 7.351 | 0.361 | 7.712 | 28.328 | 35.780 | 28.428 | 36.141 |
| Extent 1 | 0.011 | 0.012 | 0.001 | 0.001 | 0.01 | 0.011 | 0.873 | 0.862 | 0.861 | 0.872 |
| Form factor | 0.188 (***) | 0.27 (***) | 0.107 (***) | 0.082 (***) | 0.081 (***) | 0.164 (***) | 0.465 | 0.653 | 0.735 | 0.572 |
| Inner difference length | 0.459 (***) | 0.674 (***) | 0.207 (***) | 0.214 | 0.252 (***) | 0.467 (***) | 0.303 | 0.762 | 0.977 | 0.510 |
| Inner difference length (max) | 0.463 (***) | 0.692 (***) | 0.21 (***) | 0.228 | 0.254 (***) | 0.482 (***) | 0.315 | 0.778 | 1.007 | 0.524 |
| Inner protuberance length | 0.077 | 0.153 | 0.04 | 0.076 | 0.036 | 0.112 | 0.110 | 0.187 | 0.263 | 0.150 |
| Maximum wall thickness | 0.467 (***) | 0.719 (***) | 0.213 (***) | 0.252 | 0.255 (***) | 0.506 (***) | 0.394 | 0.862 | 1.113 | 0.607 |
| Mean wall thickness | 0.399 (***) | 0.61 (***) | 0.185 (***) | 0.211 | 0.213 (***) | 0.424 (***) | 0.343 | 0.741 | 0.952 | 0.528 |
| Median wall thickness | 0.439 (***) | 0.669 (***) | 0.202 (***) | 0.23 | 0.237 (***) | 0.467 (***) | 0.356 | 0.795 | 1.025 | 0.558 |
| Outer difference length | 0.008 | 0.02 | 0.004 | 0.028 | 0.012 | 0.016 | 0.017 | 0.025 | -0.003 | 0.013 |
| Outer difference length (max) | 0.096 (***) | 0.08 | 0.048 (**) | 0.015 | 0.047 (*) | 0.032 | 0.123 | 0.219 | 0.203 | 0.171 |
| Outer protuberance length | 0 | 0.015 | 0.004 | 0.015 | 0.004 | 0.011 | 0.057 | 0.057 | 0.072 | 0.061 |
| Radius ratio | 6.327 (***) | 7.331 (**) | 3.936 (***) | 1.004 | 2.391 | 3.395 | 5.889 | 12.217 | 13.220 | 9.825 |
| Rim bottom width | 0.465 (***) | 0.717 (***) | 0.21 (***) | 0.252 | 0.254 (***) | 0.507 (***) | 0.377 | 0.841 | 1.093 | 0.587 |
| Rim top flatness | 0.014 | 0.023 | 0.001 | 0.009 | 0.014 | 0.024 | 0.090 | 0.104 | 0.113 | 0.090 |
| Roundness | 0.103 (***) | 0.165 (***) | 0.056 (***) | 0.062 (***) | 0.047 (***) | 0.109 (***) | 0.210 | 0.313 | 0.375 | 0.266 |
| SD wall thickness | 0.096 (***) | 0.149 (***) | 0.043 (***) | 0.053 | 0.053 (***) | 0.106 (**) | 0.053 | 0.149 | 0.202 | 0.095 |
| Trapezoid % | 12.622 (***) | 14.318 (*) | 11.481 (***) | 1.696 | 1.141 | 2.837 | 142.240 | 154.862 | 156.558 | 153.721 |

The algorithmically defined morphological subgroups show no chronological relevance (see ***Table 10***), since three out of four peak at Phase 1, while cluster-3 captures a variant that peaks at Phase 3. As previously discussed, the latter is defined based on few members and is not very typical example of 1A130 according to the material specialist. However, the presence of these morphological groups motivates further analysis in extrinsic properties, apart from morphology and chronological interpretation, that may provide explanations for their presence. A plausible next research step is to conduct chemical analysis on the pottery fabric and slip to study the composition and provenance of the raw material. Overall, considering that this type was popular in the eastern Mediterranean with a Hellenistic precursor, it is plausible for the type to be produced in multiple workshops. Our first working hypothesis is that the morphological subgroups could be related to the presence of different workshops that procured their raw material from different areas around Sagalassos. Our second working hypothesis relates to the organization of labor in the economic system present at the time. If the system supported a horizontal organization of production, raw material could be supplied by one resource and further artisanal production was conducted by specialized artisans in different workshops. These hypotheses though remain to be tested, which goes beyond the scope of this paper.

***Table 10*** *Proportion of 1A130 profiles per cluster for each SRSW Phase*

| SRSW Phase | Cluster of Type 1A130 | | | | Profile Count (Phase) |
|---|---|---|---|---|---|
| | 1 | 2 | 3 | 4 | |
| Phase 1 | 67% | 85% | 30% | 76% | 82.5 |
| Phase 2 | 9% | 2% | 10% | 7% | 7 |
| Phase 3 | 11% | 4% | 60% | 4% | 10.2 |
| Phase 4 | 5% | 0% | 0% | 1% | 2.7 |
| Phase 5 | 5% | 0% | 0% | 10% | 6.7 |
| Phase 6 + | 3% | 9% | 0% | 2% | 4 |
| Cluster Count (Cluster) | 40 | 23 | 5 | 46 | 114 |

# Discussion and future work

Pottery classification is one of the key approaches in archaeological analysis for understanding similarities and differences in material culture. In this paper, we contributed to the existing suite of automatic, computerized typological arrangement methods, and we provided a replicable process to attribute fuzzy descriptors and fuzzy definitions to material classes. Our proposal considers traditional archaeological practices by accommodating existing theoretical modes and leaving space for expert input, while bringing greater granularity into the morphological pottery analysis and build towards the creation of coherent discourses about past societies. The proposed model is an elegant algorithmic solution to build a digital hub around a conceptual typological model, which has the potential to take up a prominent role within future core analytical approaches in digital pottery analysis. The created output can aid material experts to access legacy data, enrich, restructure, and rethink their models, discuss specific hypotheses, and update or maintain their beliefs. The proposed methodological pipeline is implemented here for the Sagalassos Archaeological Research Project but is inherently suitable for other configurations to match specific research questions of other (re)arranged typological models.

Our proposal can be considered a 'from image to numbers, and from numbers to text and discourse' approach. The digital aspects of this proposed pipeline allow detailed and well-tracked shape quantification, which is high-dimensional and precise. Multivariate comparisons and tracking of morphological characteristics offer important potential advances for the symbiosis between computational approaches and material specialists. Our proposal offers a hypotheses-generation and hypothesis-evaluation dimension, allowing interaction with and reflection on the conceptual model, where iterations can be performed to accumulate knowledge in the digital model. The method integrates archaeological reality by providing ways to work with incomplete and fragmented vessels. In general, the material specialist is called upon to infer the class based only on the rim sherd several times, since rims are in general more abundant than complete profiles and serve typically as diagnostic pieces. This is also the case in the SRSW typology.

The data generated by our digital model based on technical drawings provide input for describing and defining typological classes, and comparing the most typical cases, most atypical cases, and groupings within the shapes of *terra sigillata* tableware.

For the description of typological classes, (i) we constructed fuzzy labels based on the labels provided by the material specialist, (ii) we constructed fuzzy labels from scratch based on matching the conceptual model with geometric morphology measures, and (iii) we highlighted causality in the making of fuzzy rules where there is transparency on the indications for why a profile gets a fuzzy label. The proposed parameters are measured in centimeters for the profile aligned in a Cartesian coordinate system and they could be directly extended to any other dataset, evaluate how well they match specific characteristics or expectations of each (re)arranged typological model.

For the definition of typological classes, we created algorithmic, numerical, and visual representations that depict the typological arrangement embedded in a network graph, distinguish between central/peripheral/marginal cases and locate morphological variants within types. Our overview provides a window into the mental image of a class based on morphological variations in shape dimensions defined by the algorithmic implementation of the conceptual model. Regarding the class definition within SRSW, we analyzed profiles with plain rims since these are the most difficult when discerning types, in contrast to the pronounced rims. Extensions to pronounced rims will be considered in the future. Finally, any proper redefinition of the SRSW typology needs to incorporate the aspect of chronological salience. We tackled this aspect by relating the proposed algorithmic groups to the chronological label of each archeological locus, for each find. Our approach provides the foundation for cross-context analysis and cross-dating. The proposed grouping can be used for analyzing the relationships between contexts based on finds morphology, potential variants, and growth-peak-decline curves.

Our proposal also has certain limits. First, it does not provide results that can be directly considered socially relevant. The concept of type designation as discussed by Adams and Adams (1991) is beyond type description and type definition. In this work, we do not proceed to the level of type designation, which requires additional analysis to ascertain the archaeological utility to its full extent, and therefore do not consider the delineation of day-to-day choices of producers and consumers in ancient Sagalassos. Moreover, we have currently only transformed a portion of the polythetic rim descriptors, In the future, fuzzy descriptors for the wall and base can be constructed, and additional attention can be given to decoration patterns, grooves and hollows, using shape quantification methods.

There are additional limits with respect to the algorithmic implementation. First, we have chosen a specific grid to search for the most optimal distance metric. Our list of initial distance metric choices is not exhaustive but the algorithmic implementation in SSDM allows adding distance metrics automatically for each shape quantification method employed in the current work. Second, our approach cannot be directly applied by material specialists, as a statistical analyst is needed to operate the model. Third, the success of the algorithmic implementation to reconstruct the conceptual model depends on the available dataset, the known parameters of the model, and their alignment with the applied algorithms. Whether the parameters that define the form are the most suitable ones depends on the conceptual model, the knowledge that is accumulated by the material specialist, and the ability of the analyst to elicit and match this knowledge with algorithmic implementation taking into account the availability of the data. Next, a few iterations have been performed to explore a portion of the possibilities in eliciting the conceptual model, improve the analytical pipeline, and enrich the data from the considered digital record. A portion of the potential shape quantification methods have been explored to link profile forms with type descriptions and definitions.

We consider four main areas for further research. The first, pertains to the continued development of algorithmic implementations that capture information vagueness in typological (re)arrangement models. Fuzzy logic approaches are applicable such pottery studies, but so are statistical approaches, while a database system that supports the inclusion the created data should also be selected. We envision typological modelling approaches that incorporate information vagueness in a digital toolkit to be associated with traditional approaches in typological arrangement, not only in grouping but also in approaches such as paradigmatic and non-dimensional (taxonomy) classification, as well as bounded grouping. Also, other elicitation methods can be applied in defining membership functions when these are expected to be defined from scratch. Conducting and incorporating the results of an ethnoarchaeometric study would add to determining the conceptual model. Another important aspect of the modelling approach is to reflect on the representativity of the sample sizes and the unbiasedness of the labels attributed by material specialists, before validating whether models can be used for further research. Other extensions could also utilize fuzzy rules and soft boundaries in defining central/peripheral/marginal cases. Finally, when textual descriptions are based on class labels provided earlier, we can reflect further on the empirical probability density functions of the geometric measures per class and modify by selecting profiles that act as reference points and by excluding outliers when constructing the membership functions.

The second area of continued research is the treatment of missing data, such as the statistical imputation of profile walls that are not preserved and are therefore not available in the technical drawings. Such an approach will increase available sample sizes but also reflect better the conceptual model. Even though the material specialists may not physically inspect the part of the wall that is missing, based on their experience they can, in several cases, create a cognitive range of possibilities and mentally construct an approximate shape for the missing part. Although this may at first seem abstract, there are underlying rules that define more probable solutions than others which adhere to the mental image of the class. We may further investigate how these rules can be verbalized and contextualized in available pottery data, such that we can perform fuzzy morphological data imputation of the missing profile parts.

The third area for further research is the elaboration of the available user interface and the contribution to a linked open database system. For the user interface to be built on top of our digital model, we aim to maximize the accessibility for non-programmers, the intuitiveness of the system, and the operability when material specialists are actively using it. The data would ideally be available in accordance with standardized database structures, using controlled vocabularies and allowing alignment with other typological models of *terra sigillata*.

Finally, we consider data digitization and interoperability of algorithms within and between research projects an important aspect to be tackled by the community as a whole. There is an increasing interest in, and progress made by colleagues working in the field of digital pottery analysis, and several project-specific models and configurations already exist. A case in point is the fact that our pipeline depends on technical drawings to feed the algorithmic implementations *versus* the fact that algorithms developed by other research projects (Arch-I-Scan, ArchAIDE) depend on photos taken for each sherd in a project-specific controlled environment. This shows that for all the recent advances, the broader integration of systems and generalization of models on a discipline-wide level has not gained much progress. If we are to truly take a step towards the next level, we need to develop suitable ontologies with the desired granularity that are well-received and broadly-used by material specialists in the field. We hope that the current paper offers a well-measured step towards this goal.

## Conclusions

In this paper, we focused on the morphological features of archaeological pottery and provided a more solid basis for analytical methods designed to construct and rethink typologies. The proposed methodology deals with complex legacy data, gives new visual and analytical perspectives to typological arrangements while making grouping and description explicit. This work can only be considered work in progress since so far only a fraction of possibilities has been studied. Nevertheless, the provided range of data creation, modelling, and visualization possibilities, contributes to conducting a systematic conceptual analysis in an algorithmic fashion and connects fuzzy logic with the use of polythetic descriptors and the ambivalence of typological grouping and classification.

For fuzzy descriptions created from scratch, we make an effort to incorporate prior implicit archaeological logic in forming rules that revolve around the same rationale and terminology of morphological detail, whilst not being based on specific types. For fuzzy descriptors created based on previously attributed labels, we provided a standardized approach to automatically translate crisp labels to fuzzy, incorporating the vagueness that a typological model always contains. These approaches are of importance not only for SRSW, but for all morphologically developed tablewares, be these *terra sigillata*, red slip wares or other non-Roman tablewares with a relatively high number of forms for specific functions that tend to follow some kind of fashion and change over time.

The digital model clearly adds to the archaeological methods, and provides access to facts and numbers to clarify or answer earlier hunches or open questions. When a typological model is constructed and followed throughout many years of archaeological research, certain trends are observed and hypotheses about the implications of these trends may be created. In such cases, the proposed approach built on fuzzy type definition can be used to test these hypotheses and identify whether the cognitively inferred trends are verified by the data, based on systematized form analyses in connection to fuzzy logic and statistical protocols.

## Acknowledgements

The authors acknowledge the contribution of Philip Bes for data collection and reflection on pottery analysis, Dries Daems for reflection on pottery analysis and proofreading, Eliane Mahy for the digitization of paper drawings. The authors also thank Margo Van Steenlandt and Thor Deyaert for assisting in drawings retrieval and metadata recording, and finally all the excavation, depot and illustration teams involved in the Sagalassos excavation campaigns throughout the years 1992 – 2022.

## Declarations

### Funding

This work was supported by the Research Foundation – Flanders and the Research Fund of KU Leuven.

### Data availability

Data generated and analyzed during the current study are available from the corresponding author on reasonable request.

### Code availability

The scripts to retrieve shape quantifications and perform fuzzy typological arrangement are available open access in (Kafetzaki, 2022a). The scripts to obtain the shiny app are available open access in (Kafetzaki, 2022b). The scripts to perform statistical selection of distance metric are available open access in (Kafetzaki, 2023).

### Competing Interests

The authors have no competing interests to declare that are relevant to the content of this article.

## References

Adams, W. Y., & Adams, E. W. (1991). *Archaeological typology and practical reality. A Dialectical Approach to Artifact Classification and Sorting.*

Albero, S. D., Calvo, T. M., & Garcia, R. J. (2016). Formal Analysis and Typological Classification in the Study of Ancient Pottery. In A. Hunt (Ed.), *The Oxford Handbook of Archaeological Ceramic Analysis* (pp. 181–199).

Alcaide, D., & Aerts, J. (2020). Spanning Trees as Approximation of Data Structures. *IEEE Transactions on Visualization and Computer Graphics*, 1–1. https://doi.org/10.1109/TVCG.2020.2995465

Angelov, P. P., & Gu, X. (2018). Empirical Fuzzy Sets. *International Journal of Intelligent Systems*, *33*(2), 362–395. https://doi.org/10.1002/int.21935

Anichini, F., Dershowitz, N., Dubbini, N., Gattiglia, G., Itkin, B., & Wolf, L. (2021). The automatic recognition of ceramics from only one photo: The ArchAIDE app. *Journal of Archaeological Science: Reports*, *36*, 102788. https://doi.org/10.1016/j.jasrep.2020.102788

Anichini, F., Francesco Banterle, Garrigós, J. B. i, Callieri, M., Dershowitz, N., Dubbini, N., Diaz, D. L., Evans, T., Gattiglia, G., Green, K., Gualandi, M. L., Hervas, M. A., Itkin, B., Fernandez, M. M. i, Gascón, E. M., Remmy, M., Richards, J., Scopigno, R., Vila, L., … Zallocco, M. (2020). Developing the ArchAIDE Application: A digital workflow for identifying, organising and sharing archaeological pottery using automated image recognition. *Internet Archaeology*, *52*. https://doi.org/10.11141/ia.52.7

Banning, E. B. (2020). *The Archaeologist's Laboratory.* Springer International Publishing.

Barceló, J. A. (1996). *Heuristic classification and fuzzy sets. New tools for archaeological typologies*.

Baxter, M. J. (2009). ARCHAEOLOGICAL DATA ANALYSIS AND FUZZY CLUSTERING. *Archaeometry*, *51*(6), 1035–1054. https://doi.org/10.1111/j.1475-4754.2008.00449.x

Bezdek, J. C. (2013). *Pattern Recognition with Fuzzy Objective Function Algorithms*. Springer Science & Business Media.

Bilgiç, T., & Türkşen, I. B. (2000). Measurement of Membership Functions: Theoretical and Empirical Work. In D. Dubois & H. Prade (Eds.), *Fundamentals of Fuzzy Sets* (Vol. 7, pp. 195–227). Springer US. https://doi.org/10.1007/978-1-4615-4429-6_4

Bouchon-Meunier, B., Dotoli, M., & Maione, B. (1996). On the choice of membership functions in a mamdani-type fuzzy controller. *Citeseer*, 7.

Caliński, T., & Harabasz, J. (1974). A dendrite method for cluster analysis. *Communications in Statistics*, *3*(1), 1–27. https://doi.org/10.1080/03610927408827101

Calliari, I., Canal, E., Cavazzoni, S., & Lazzarini, L. (2001). Roman bricks from the Lagoon of Venice: A chemical characterization with methods of multivariate analysis. *Journal of Cultural Heritage*, *2*(1), 23–29. https://doi.org/10.1016/S1296-2074(01)01110-4

Caple, J. (2017). Elliptical Fourier analysis: Fundamentals, applications, and value for forensic anthropology. *Int J Legal Med*, 16.

Cardillo, M. (2010). Some Applications of Geometric Morphometrics to Archaeology. In A. M. T. Elewa (Ed.), *Morphometrics for Nonmorphometricians* (pp. 325–341). Springer. https://doi.org/10.1007/978-3-540-95853-6_15

Carlo, J. M., Barbeitos, M. S., & Lasker, H. R. (2011). Quantifying Complex Shapes: Elliptical Fourier Analysis of Octocoral Sclerites. *The Biological Bulletin*, *220*(3), 224–237. https://doi.org/10.1086/BBLv220n3p224

Chambers, J. M., Freeny, A. E., & Heiberger, R. M. (1992). Analysis of Variance; Designed Experiments. In *Statistical Models in S* (1st ed.). Routledge.

Chang, W., Cheng, J., Allaire, J., Xie, Y., & McPherson, J. (2020). *shiny: Web Application Framework for R* (R package version 1.4.0.2) [Computer software]. https://CRAN.R-project.org/package=shiny

Christmas, J., & Pitts, M. (2018). Classifying and Visualising Roman Pottery using Computer-scanned Typologies. *Internet Archaeology*, *50*. https://doi.org/10.11141/ia.50.14

Cintas, C., Lucena, M., Fuertes, J. M., Delrieux, C., Navarro, P., González-José, R., & Molinos, M. (2020). Automatic feature extraction and classification of Iberian ceramics based on deep convolutional networks. *Journal of Cultural Heritage*, *41*, 106–112. https://doi.org/10.1016/j.culher.2019.06.005

Daems, D., & Poblome, J. (2022). The Hellenistic pottery of Sagalassos: A Typological Update. *Manufacturers and Markets: The Contributions of Hellenistic Pottery to Economies Large and Small*, *4*, 607–617.

Daems, D., van der Enden, M., Poblome, J., & Talloen, P. (2019). The Hellenistic pottery repertoire made at Sagalassos, SW Anatolia. *Daily Life in a Cosmopolitan World. Pottery and Culture During the Hellenistic Period*, *2*, 81–96.

De Leeuw, J., & Mair, P. (2015). Shepard diagram. In N. Balakrishnan, T. Colton, B. Everitt, W. Piegorsch, F. Ruggeri, & J. L. Teugels (Eds.), *Wiley StatsRef: Statistics Reference Online* (1st ed.). Wiley. https://doi.org/10.1002/9781118445112

Dijkstra, E. W. (1959). A Note on Two Problems in Connexion with Graphs. *Numerische Mathematik*, *1*, 269–271.

Dubois, D. (2006). Possibility theory and statistical reasoning. *Computational Statistics & Data Analysis*, *51*(1), 47–69. https://doi.org/10.1016/j.csda.2006.04.015

Dubois, D., & Prade, H. (1988). *Possibility theory: An approach to computerized processing of uncertainty* (Vol. 41). Plenum Press. https://onlinelibrary.wiley.com/doi/10.1002/(SICI)1097-4571(199003)41:2<153::AID-ASI16>3.0.CO;2-U

Dubois, D., & Prade, H. (2015). Possibility Theory and Its Applications: Where Do We Stand? In J. Kacprzyk & W. Pedrycz (Eds.), *Handbook of Computational Intelligence* (p. 30). Springer.

Dubois, D., & Prade, H. (2021). Membership Functions. In M.-J. Lesot & C. Marsala (Eds.), *Fuzzy Approaches for Soft Computing and Approximate Reasoning: Theories and Applications* (Vol. 394, pp. 5–20). Springer International Publishing. https://doi.org/10.1007/978-3-030-54341-9

Duistermaat, K. (2016). The Organization of Pottery Production: Toward a Relational Approach. In *Oxford handbooks series* (pp. 114–147). Oxford University Press. https://doi.org/10.1093/oxfordhb/9780199681532.013.9

Dunn, J. C. (1973). A Fuzzy Relative of the ISODATA Process and Its Use in Detecting Compact Well-Separated Clusters. *Journal of Cybernetics*, *3*(3), 32–57. https://doi.org/10.1080/01969727308546046

Dunn, O. J. (1964). Multiple Comparisons Using Rank Sums. *Technometrics*, *6*(3), 241–252. https://doi.org/10.1080/00401706.1964.10490181

Dunnell, R. C. (1971). *Systematics in prehistory*. New York: The Free Press.

Fox, J. (2015). *Applied Regression Analysis and Generalized Linear Models*. SAGE Publications.

Fox, J., & Weisberg, S. (2018). *An R Companion to Applied Regression*. SAGE Publications.

Frey, B. J., & Dueck, D. (2007). Clustering by Passing Messages Between Data Points. *Science*. https://doi.org/10.1126/science.1136800

Gansell, A. R., Meent, J.-W. van de, Zairis, S., & Wiggins, C. H. (2014). Stylistic clusters and the Syrian/South Syrian tradition of first-millennium BCE Levantine ivory carving: A machine learning approach. *Journal of Archaeological Science*, *44*, 194–205. https://doi.org/10.1016/j.jas.2013.11.005

Garibaldi, J. M., & John, R. I. (2003). Choosing membership functions of linguistic terms. *The 12th IEEE International Conference on Fuzzy Systems, 2003. FUZZ ’03.*, 578–583. https://doi.org/10.1109/FUZZ.2003.1209428

Garibaldi, J. M., Musikasuwan, S., Ozen, T., & John, R. I. (2004). A case study to illustrate the use of non-convex membership functions for linguistic terms. *2004 IEEE International Conference on Fuzzy Systems (IEEE Cat. No.04CH37542)*, *3*, 1403–1408. https://doi.org/10.1109/FUZZY.2004.1375377

Gero, J., & Mazzullo, J. (1984). Analysis of Artifact Shape Using Fourier Series in Closed Form. *Journal of Field Archaeology*, *11*(3), 315–322. https://doi.org/10.1179/009346984791535467

Gilboa, A., Karasik, A., Sharon, I., & Smilansky, U. (2004). Towards computerized typology and classification of ceramics. *Journal of Archaeological Science*, *31*(6), 681–694. https://doi.org/10.1016/j.jas.2003.10.013

Green, D. F. (1975). Testing a traditional typology using cluster analysis. *Proceedings Annual Conference on Computer Applications in Archaeology*, 25–32.

Gualandi, M. L., Gattiglia, G., & Anichini, F. (2021). An Open System for Collection and Automatic Recognition of Pottery through Neural Network Algorithms. *Heritage*, *4*(1), 140–159. https://doi.org/10.3390/heritage4010008

Hardy-Smith, A. (1974). Post-medieval pot shapes: A quantitative analysis. *Science and Archaeology*, *11*, 4–15.

Harris, T. R., Stoddard, S. W., & Bezdek, J. C. (1993). Application of Fuzzy-Set Clustering for Regional Typologies. *Growth and Change*, *24*(2), 155–165. https://doi.org/10.1111/j.1468-2257.1993.tb00958.x

Hastie, T., & Tibshirani, R. (1986). Generalized Additive Models. *Statisical Science*, *1*(3), 297–318.

Hayes, J. W. (1991). *The Hellenistic and Roman Pottery [Paphos]: By JW Hayes*. Department of Antiquities, Cyprus.

Hermon, S., & Niccolucci, F. (2002). A fuzzy logic approach to typology in archaeological research. *The Digital Heritage of Archaeology: CAA*, 307–310.

Hermon, S., Niccolucci, F., Alhaique, F., Iovino, M.-R., & Leonini, V. (2004). Archaeological typologies-an archaeological fuzzy reality. *BAR International Series*, *1227*, 5.

High-Steskal, N., Rembart, L., & Katzjäger, D. (2019). *Terminology for the description of the shape of pottery fragments from Hellenistic and Roman contexts*. https://zenodo.org/record/3442243

Hinton, G., & Roweis, S. (2002). *Stochastic Neighbor Embedding*.

Hoggard, C. S., McNabb, J., & Cole, J. N. (2019). The Application of Elliptic Fourier Analysis in Understanding Biface Shape and Symmetry Through the British Acheulean. *Journal of Paleolithic Archaeology*, *2*(2), 115–133. https://doi.org/10.1007/s41982-019-00024-6

Hollander, M., Wolfe, D. A., & Chicken, E. (2013). *Nonparametric Statistical Methods*. John Wiley & Sons.

Kafetzaki, D. (2022a). *Morphotype* (0.1.0) [Computer software]. Zenodo. https://doi.org/10.5281/zenodo.6760148

Kafetzaki, D. (2022b). *MorphotypeShiny* (0.1.0) [Computer software]. Zenodo. https://doi.org/10.5281/zenodo.6760607

Kafetzaki, D. (2023). *SSDM* (0.1.0) [Computer software]. Zenodo. https://doi.org/10.5281/zenodo.8025851

Kampel, M., & Sablatnig, R. (2007). Rule based system for archaeological pottery classification. *Pattern Recognition Letters*, *28*(6), 740–747. https://doi.org/10.1016/j.patrec.2006.08.011

Karasik, A., & Smilansky, U. (2011). Computerized morphological classification of ceramics. *Journal of Archaeological Science*, *38*(10), 2644–2657. https://doi.org/10.1016/j.jas.2011.05.023

Karasik, A., Smilansky, U., & Beit-Arieh, I. (2005). New Typological Analyses of Early Bronze Age Holemouth Jars from Tel Arad and Southern Sinai. *Tel Aviv*, *32*(1), 20–31. https://doi.org/10.1179/tav.2005.2005.1.20

Karl, S., Houska, P., Lengauer, S., Haring, J., Trinkl, E., & Preiner, R. (2022). Advances in digital pottery analysis. *It - Information Technology*, *0*(0). https://doi.org/10.1515/itit-2022-0006

Kaufman, L., & Rousseeuw, P. J. (2009). *Finding Groups in Data: An Introduction to Cluster Analysis*. John Wiley & Sons.

Kempton, W. (1981). *The Folk Classification of Ceramics: A Study of Cognitive Prototypes*. Elsevier.

Klir, G. J. (1999). On fuzzy-set interpretation of possibility theory. *Fuzzy Sets and Systems*, *108*(3), 263–273. https://doi.org/10.1016/S0165-0114(97)00371-0

Kobylinski, Z., & Buko, A. (1992). Computer clustering in the analysis of non-morphological attributes of pottery sherds: Two examples from Poland. *Computing the Past. Computer Applications and Quantitative Methods in Archaeology CAA92*, 349–356.

Kowalczyk, R. (1998). On linguistic approximation of subnormal fuzzy sets. *1998 Conference of the North American Fuzzy Information Processing Society - NAFIPS (Cat. No.98TH8353)*, 329–333. https://doi.org/10.1109/NAFIPS.1998.715600

Kowalczyk, R. (1999). On numerical and linguistic quantification in linguistic approximation. *IEEE SMC'99 Conference Proceedings. 1999 IEEE International Conference on Systems, Man, and Cybernetics (Cat. No.99CH37028)*, *5*, 326–331. https://doi.org/10.1109/ICSMC.1999.815570

Kurnianggoro, L., Wahyono, & Jo, K.-H. (2018). A survey of 2D shape representation: Methods, evaluations, and future research directions. *Neurocomputing*, *300*, 1–16. https://doi.org/10.1016/j.neucom.2018.02.093

Lai Chung, F., & Lee, T. (1994). Fuzzy competitive learning. *Neural Networks*, *7*(3), 539–551. https://doi.org/10.1016/0893-6080(94)90111-2

Leese, M. N., & Main, P. L. (1983). An approach to the assessment of artefact dimension as descriptors of shape. *Computer Applications in Archaeology*, 171–180.

Lenardi, M. J., & Merwin, D. E. (2010). Towards Automating Artifact Analysis: A Study Showing Potential Applications of Computer Vision and Morphometrics to Artifact Typology. In A. M. T. Elewa (Ed.), *Morphometrics for Nonmorphometricians* (pp. 289–305). Springer. https://doi.org/10.1007/978-3-540-95853-6_13

Lestrel, P. E., CESAR Jr., R. M., Takahashi, O., & Kanazawa, E. (2004). A Fourier-wavelet representation of 2-D shapes: Sexual dimorphism in the Japanese cranial base. *Anthropological Science*, *112*(1), 3–28. https://doi.org/10.1537/ase.00069

Li, M., An, H., Angelovici, R., Bagaza, C., Batushansky, A., Clark, L., Coneva, V., Donoghue, M. J., Edwards, E., Fajardo, D., Fang, H., Frank, M. H., Gallaher, T., Gebken, S., Hill, T., Jansky, S., Kaur, B., Klahs, P. C., Klein, L. L., … Chitwood, D. H. (2018). Topological Data Analysis as a Morphometric Method: Using Persistent Homology to Demarcate a Leaf Morphospace. *Frontiers in Plant Science*, *9*, 553. https://doi.org/10.3389/fpls.2018.00553

Liming, G., Hongjiet, L., & Wilcockî, J. (1989). *The analysis of ancient Chinese pottery and porcelain shapes: A study of classical profiles from the Yangshao culture to the Qing dynasty using computerised profile data reduction , cluster analysis and fuzzy boundary discrimination*. 362–374. /paper/The-analysis-of-ancient-Chinese-pottery-and-shapes-Li-ming-Hongjiet/d9d6a82b2090ac4a2cd1544bff57758353ad7906

Lo Buglio, D., Lardinois, V., & De Luca, L. (2013). Revealing shape semantics from morphological similarities of a collection of architectural elements: The case study of the columns of Saint-Michel de Cuxa. *2013 Digital Heritage International Congress (DigitalHeritage)*, 465–472. https://doi.org/10.1109/DigitalHeritage.2013.6743785

Lucena, M., Fuertes, J. M., Martínez-Carrillo, A. L., Ruiz, A., & Carrascosa, F. (2017). Classification of archaeological pottery profiles using modal analysis. *Multimedia Tools and Applications*, *76*(20), 21565–21577. https://doi.org/10.1007/s11042-016-4076-9

Lucena, M., Martínez-Carrillo, A. L., Fuertes, J. M., Carrascosa, F., & Ruiz, A. (2016). Decision support system for classifying archaeological pottery profiles based on Mathematical Morphology. *Multimedia Tools and Applications*, *75*(7), 3677–3691. https://doi.org/10.1007/s11042-014-2063-6

Main, P. L. (1987). Accessing outline shape information efficiently within a large database II: database compaction techniques. *Computer and Quantitative Methods in Archaeology*, *1987*, 243–251.

Martínez-Carrillo, A. L., Lucena, M. J., Fuertes, J. M., & Ruiz, A. (2010). Morphometric Analysis Applied to the Archaeological Pottery of the Valley of Guadalquivir. In A. M. T. Elewa (Ed.), *Morphometrics for Nonmorphometricians* (pp. 307–323). Springer. https://doi.org/10.1007/978-3-540-95853-6_14

Martin-Rodilla, P., & Gonzalez-Perez, C. (2019). Conceptualization and Non-Relational Implementation of Ontological and Epistemic Vagueness of Information in Digital Humanities. *Informatics*, *6*(2), 20. https://doi.org/10.3390/informatics6020020

McInnes, L., Healy, J., & Melville, J. (2020). UMAP: Uniform Manifold Approximation and Projection for Dimension Reduction. *ArXiv:1802.03426 [Cs, Stat]*. http://arxiv.org/abs/1802.03426

Meyza, H. (2007). *Nea Paphos. 5, Cypriot red slip ware: Studies on a late Roman Levantine fine ware*.

Migliorini, S., Quintarelli, E., & Belussi, A. (2022). Tracking Data Provenance of Archaeological Temporal Information in Presence of Uncertainty. *Journal on Computing and Cultural Heritage*, *15*(2), 1–32. https://doi.org/10.1145/3480956

Mingqiang, Y., Kidiyo, K., & Joseph, R. (2008). A Survey of Shape Feature Extraction Techniques. *Pattern Recognition*, *15*(7), 43–90.

Navarro, P., Cintas, C., Lucena, M., Fuertes, J. M., Delrieux, C., & Molinos, M. (2021). Learning feature representation of Iberian ceramics with automatic classification models. *Journal of Cultural Heritage*, 9.

Neal, F. B., & Russ, J. C. (2012). *Measuring shape*. CRC Press.

Niccolucci, F., D'Andrea, A., & Crescioli, M. (2001). Archaeological applications of fuzzy databases. *BAR INTERNATIONAL SERIES*, *931*, 107–116.

Niccolucci, F., & Hermon, S. (2015). Time, Chronology and Classification. In J. A. Barcelo & I. Bogdanovic (Eds.), *Mathematics and Archaeology*. CRC Press.

Orton, C. (1982). *Mathematics in archaeology*. Cambridge University Press Cambridge.

Orton, C., Hughes, M., & Hughes, M. (2013). *Pottery in Archaeology*. Cambridge University Press.

Pal, N. R., Bezdek, J. C., & Hathaway, R. J. (1996). Sequential Competitive Learning and the Fuzzy c-Means Clustering Algorithms. *Neural Networks*, *9*(5), 787–796. https://doi.org/10.1016/0893-6080(95)00094-1

Pappis, C. P., & Siettos, C. I. (2014). Fuzzy reasoning. In *Search methodologies* (pp. 519–556). Springer.

Parisotto, S., Leone, N., Schönlieb, C.-B., & Launaro, A. (2022). Unsupervised clustering of Roman potsherds via Variational Autoencoders. *Journal of Archaeological Science*, *142*, 105598. https://doi.org/10.1016/j.jas.2022.105598

Pau, G., Fuchs, F., Sklyar, O., Boutros, M., & Huber, W. (2010). EBImage—An R package for image processing with applications to cellular phenotypes. *Bioinformatics*, *26*(7), 979–981. https://doi.org/10.1093/bioinformatics/btq046

Pavlidis, T. (1978). A review of algorithms for shape analysis. *Computer Graphics and Image Processing*, *7*(2), 243–258. https://doi.org/10.1016/0146-664X(78)90115-6.

Pawlowicz, L. M., & Downum, C. E. (2021). Applications of deep learning to decorated ceramic typology and classification: A case study using Tusayan White Ware from Northeast Arizona. *Journal of Archaeological Science*, *130*, 105375. https://doi.org/10.1016/j.jas.2021.105375

Pearson, K. (1901). LIII. On lines and planes of closest fit to systems of points in space. *The London, Edinburgh, and Dublin Philosophical Magazine and Journal of Science*, *2*(11), 559–572. https://doi.org/10.1080/14786440109462720

Poblome, J. (1999). *Sagalassos red slip ware: Typology and chronology*. Brepols.

Poblome, J. (2016). The Potters of Ancient Sagalassos Revisited. In A. Wilson & M. Flohr (Eds.), *Urban Craftsmen and Traders in the Roman World* (pp. 377–404). Oxford University Press. https://doi.org/10.1093/acprof:oso/9780198748489.003.0017

Poblome, J., & Bes, P. (2018). This is how we do it. Methodology of pottery processing at Sagalassos. *Rei Cretariae Romanae Favtorvm Acta*, *45*, 731–740.

Poblome, J., Bes, P., De Cupere, B., Lauwers, V., Kerlijne, R., Vionis, A., & Waelkens, M. (2010). Sic transit gloria mundi. Does it really? Wasting seventh century AD Sagalassos (SW Turkey). In S. Menchelli, S. Santoro, M. Pasquinucci, & G. Guiducci (Eds.), *LRCW3. Late Roman Coarse Wares, Cooking Wares and Amphorae in the Mediterranean: Archaeology and archaeometry. Comparison between western and eastern Mediterranean* (Vol. 2185, pp. 791–801). Archaeobooks; Oxford. https://doi.org/10.30861/9781407300986

Pota, M., Esposito, M., & De Pietro, G. (2013). Transforming probability distributions into membership functions of fuzzy classes: A hypothesis test approach. *Fuzzy Sets and Systems*, *233*, 52–73. https://doi.org/10.1016/j.fss.2013.03.013

Pota, M., Esposito, M., & De Pietro, G. (2018). Likelihood-fuzzy analysis: From data, through statistics, to interpretable fuzzy classifiers. *International Journal of Approximate Reasoning*, *93*, 88–102. https://doi.org/10.1016/j.ijar.2017.10.022

R Core Team. (2020). *R: A Language and Environment for Statistical Computing*. R Foundation for Statistical Computing. https://www.R-project.org/

Read, D. W. (2007). *Artifact classification: A conceptual and methodological approach*. Left Coast Press.

Rice, P. M. (2015). *Pottery Analysis, Second Edition: A Sourcebook*. University of Chicago Press.

Rosch, E. (1975). Cognitive reference points. *Cognitive Psychology*, *7*(4), 532–547. https://doi.org/10.1016/0010-0285(75)90021-3

Rovner, I. (1995). Complex measurements made easy: Morphometric analysis of artefacts using Expert Vision Systems. *BAR INTERNATIONAL SERIES*, *598*, 7.

Royston, J. P. (1982a). Algorithm AS 181: The W Test for Normality. *Journal of the Royal Statistical Society. Series C (Applied Statistics)*, *31*(2), 176–180. https://doi.org/10.2307/2347986

Royston, J. P. (1982b). An Extension of Shapiro and Wilk's W Test for Normality to Large Samples. *Journal of the Royal Statistical Society. Series C (Applied Statistics)*, *31*(2), 115–124. https://doi.org/10.2307/2347973

RStudio Team. (2016). *RStudio: Integrated Development Environment for R*. RStudio, Inc. http://www.rstudio.com/

Runz, C. D., Desjardin, E., Piantoni, F., & Herbin, M. (2007). USING FUZZY LOGIC TO MANAGE UNCERTAIN MULTI-MODAL DATA IN AN ARCHAEOLOGICAL GIS. *Nternational Symposium on Spatial Data Quality-ISSDQ*, *7*, 4.

Saragusti, I., Karasik, A., Sharon, I., & Smilansky, U. (2005). Quantitative analysis of shape attributes based on contours and section profiles in artifact analysis. *Journal of Archaeological Science*, *32*(6), 841–853. https://doi.org/10.1016/j.jas.2005.01.002

Scott, R., & Whalen, T. (2000). Linguistic approximation of nonconvex membership functions using '...Except...' or '...Or...' *PeachFuzz 2000. 19th International Conference of the North American Fuzzy Information Processing Society - NAFIPS (Cat. No.00TH8500)*, 388–391. https://doi.org/10.1109/NAFIPS.2000.877458

Smith, N. G., Karasik, A., Narayanan, T., Olson, E. S., Smilansky, U., & Levy, T. E. (2014). The Pottery Informatics Query Database: A New Method for Mathematic and Quantitative Analyses of Large Regional Ceramic Datasets. *Journal of Archaeological Method and Theory*, *21*(1), 212–250. https://doi.org/10.1007/s10816-012-9148-1

Tibshirani, R., Walther, G., & Hastie, T. (2001). Estimating the number of clusters in a data set via the gap statistic. *Journal of the Royal Statistical Society*, *63*(2), 411–423.

Türkşen, I. B. (1991). Measurement of membership functions and their acquisition. *Fuzzy Sets and Systems*, *40*(1), 5–38. https://doi.org/10.1016/0165-0114(91)90045-R

Tyukin, I., Sofeikov, K., Levesley, J., Gorban, A. N., Allison, P., & Cooper, N. J. (2018). Exploring Automated Pottery Identification [Arch-I-Scan]. *Internet Archaeology*, *50*. https://doi.org/10.11141/ia.50.11

van der Enden, M., Poblome, J., & Bes, P. (2018). Sagalassian Mastoi in an Eastern Mediterranean Context. *9th Scientific Meeting on Hellenistic Pottery*, 925–945.

Van Der Maaten, L., Lange, G., & Boon, P. (2005). Visualization and Automatic Typology Construction of Pottery Profiles. *Pattern Recognition Letters*, *2614*, 2174–2186.

Wang, L.-Y., & Marwick, B. (2020). Standardization of ceramic shape: A case study of Iron Age pottery from northeastern Taiwan. *Journal of Archaeological Science: Reports*, *33*, 102554. https://doi.org/10.1016/j.jasrep.2020.102554

Webster, G. (1964). *Romano-British Coarse Pottery: A Students Guide (Council for British Archaeology Research Report 6)*.

Wenstop, F. (1976). Deductive verbal models of organizations. *International Journal of Man-Machine Studies*, *8*(3), 19.

Whalen, T., & Schott, B. (2001). Empirical comparison of techniques for linguistic approximation. *Proceedings Joint 9th IFSA World Congress and 20th NAFIPS International Conference (Cat. No. 01TH8569)*, *1*, 93–97. https://doi.org/10.1109/NAFIPS.2001.944233

Whallon, R. (1972). A New Approach to Pottery Typology. *American Antiquity*, *37*(1), 13–33. https://doi.org/10.2307/278883

Wilcock, J. D. (1974). The facilities of the PLUTARCH system. *Science and Archaeology*, *11*, 16–24.

Wilcock, J., & Shennan, S. (1975). The computer analysis of pottery shapes with application to bell beaker pottery. *Proceedings Annual Conference on Computer Applications in Archaeology*, 9.

Yandell, B. (2017). *Practical Data Analysis for Designed Experiments*. Routledge.

Zadeh, A. L. (1965). Fuzzy sets. *Information Control*, *8*(3), 338–353.

Zadeh, L. A. (1973). Outline of a New Approach to the Analysis of Complex Systems and Decision Processes. *IEEE Transactions on Systems, Man, and Cybernetics*, *SMC-3*(1), 28–44. https://doi.org/10.1109/TSMC.1973.5408575

Zadeh, L. A. (1978). FUZZY SETS AS A BASIS FOR A THEORY OF POSSIBILITY. *Fuzzy Sets and Systems*, *1*, 26.

# Appendix

*Table 11* *Full profiles of the type 1B150 labelled as cups instead of bowls from the FIS*

| ID | Profile | Cluster | Fuzzy FG set | Reason of mismatch |
|---|---|---|---|---|
| SADR010901 | 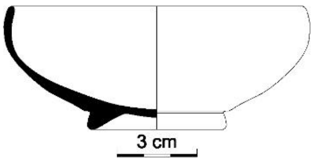 | 3 | $\left\{\frac{0.4}{cup},\frac{0.12}{bowl},\frac{0}{dish},\frac{0}{plate},\frac{0.003}{container}\right\}$ | Wall thickness at 2/3 of the height |
| SADR021195 | 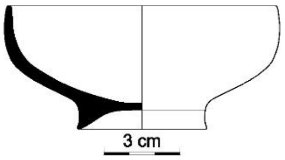 | 2 | $\left\{\frac{0.59}{cup},\frac{0.21}{bowl},\frac{0}{dish},\frac{0}{plate},\frac{0.04}{container}\right\}$ | Height/Width |